

Article

Aerosol Characterization of Northern China and Yangtze River Delta Based on Multi-Satellite Data: Spatiotemporal Variations and Policy Implications

Kuifeng Luan ^{1,2}, Zhaoxiang Cao ^{1,*}, Song Hu ¹, Zhengze Qiu ^{1,2}, Zhenhua Wang ³, Wei Shen ^{1,3} and Zhonghua Hong ³¹ College of Marine Sciences, Shanghai Ocean University, Shanghai 201306, China² Estuarine and Oceanographic Mapping Engineering Research Center of Shanghai, Shanghai 200123, China³ College of Information Science, Shanghai Ocean University, Shanghai 201306, China

* Correspondence: sunczx0210@163.com; Tel.: +86-138-3437-9296

Abstract: Horizontal and vertical distributions of aerosol properties in the Taklimakan Desert (TD), North central region of China (NCR), North China Plain (NCP), and Yangtze River Delta (YRD) were investigated by statistical analysis using Cloud-Aerosol Lidar and Infrared Pathfinder Satellite Observation (CALIPSO) L3 data from 2007 to 2020, to identify the similarities and differences in atmospheric aerosols in different regions, and evaluate the impact of pollution control policies developed in China in 2013 on aerosol properties in the study area. The aerosol optical depth (AOD) distribution had substantial seasonal and spatial distribution characteristics. AOD had high annual averages in TD (0.38), NCP (0.49), and YRD (0.52). However, these rates showed a decline post-implementation of the long-term pollution control policies; AOD values declined by 5%, 13.8%, 15.5%, and 23.7% in TD, NCR, NCP, and YRD respectively when comparing 2014–2018 to 2007–2013, and by 7.8%, 11.5%, 16%, and 10.4% when comparing 2019–2020 to 2014–2018. The aerosol extinction coefficient showed a clear regional pattern and a tendency to decrease gradually as height increased. Dust and polluted dust were responsible for the changes in AOD and extinction coefficients between TD and NCR and NCP and YRD, respectively. In TD, with change of longitude, dust aerosol first increased and then decreased gradually, peaking in the middle. Similarly in NCP, polluted dust aerosol first increased and then decreased, with a maximum value in the middle. The elevated smoke aerosols of NCP and YRD were significantly higher than those observed in TD and NCR. The high aerosol extinction coefficient values ($>0.1 \text{ km}^{-1}$) were mainly distributed below 4 km, and the relatively weak aerosol extinction coefficients ($>0.001 \text{ km}^{-1}$) were mainly distributed between 5–8 km, indicating that the high-altitude long-range transport of TD and NCR dust aerosols affects NCP and YRD.

Keywords: CALIPSO; AOD; extinction coefficient; aerosol type; temporal and spatial distribution trend; vertical distribution

Citation: Luan, K.; Cao, Z.; Hu, S.; Qiu, Z.; Wang, Z.; Shen, W.; Hong, Z. Aerosol Characterization of Northern China and Yangtze River Delta Based on Multi-Satellite Data: Spatiotemporal Variations and Policy Implications. *Sustainability* **2023**, *15*, 2029. <https://doi.org/10.3390/su15032029>

Academic Editors: Chao Chen, Jinsong Chen, Juhua Luo and Lei Fang

Received: 29 November 2022

Revised: 5 January 2023

Accepted: 12 January 2023

Published: 20 January 2023



Copyright: © 2023 by the authors. Licensee MDPI, Basel, Switzerland. This article is an open access article distributed under the terms and conditions of the Creative Commons Attribution (CC BY) license (<https://creativecommons.org/licenses/by/4.0/>).

1. Introduction

Atmospheric aerosols are usually composed of liquid droplets, solid particles, or a mixture of both suspended in the air. The main sources include natural emissions such as fine ash, dust, volcanic eruptions, and salt particles evaporated from seawater, as well as human activities such as fuel combustion, transportation, and industrial emissions [1,2]. Aerosols are an important component of Earth's atmosphere and affect the radiative forcing of solar radiation energy received at the Earth surface [3–5]. Factors such as optical properties, types, and vertical distribution of aerosols are important for the study of global and local climate change.

Furthermore, the optical properties of aerosols such as extinction coefficients and optical thickness are essential for estimating the radiative forcing of aerosol particles on the atmosphere and their impact on air quality [6].

Aerosol extinction coefficient allows us to understand how aerosols affect weather and climate [7], while aerosol optical depth (AOD) is a measurement of the extinction effect of aerosol on light, which can be calculated by the integration of aerosol extinction coefficient in the vertical direction and can be used as an approximate indicator of the degree of pollution present in the regional atmosphere [8,9]. Information on the vertical distribution of aerosols is important for a more complete understanding of aerosol behaviors such as emission, transport, movement, and transformation. Moreover, the imprecise nature of aerosol vertical information is one of the important factors contributing to the uncertainty of direct radiative forcing of aerosols [10,11]. The properties of different types of aerosols vary widely [12]. Scattering aerosols, such as sulfate aerosols, are hygroscopic and reduce the solar radiation incident to the ground-air system. In contrast, absorbing aerosols, including black- and organic carbon as well as mineral dust, have a significant heating effect on the atmosphere, leading not only to a reduction in snow and ice albedo, but also possibly water droplet evaporation and cloud cover [13,14]. Therefore, the study of aerosol types, as well as their optical properties and vertical distribution is of great scientific importance.

Satellite remote sensing can measure and note aerosol properties over long time periods and on a large scale [15,16]. Consequently, it has become a valuable tool for studying global and local climate change. Currently, methods for obtaining aerosol properties based on remote sensing technology are mainly divided into passive optical- and active remote sensing [17]. Commonly used satellite-based passive sensors for acquiring aerosol properties are the Moderate-resolution Imaging Spectroradiometer (MODIS), Visible Infrared Imaging Radiometer Suite (VIIRS), Ozone Monitoring Instrument (OMI), and the Multi-angle Imaging Spectro Radiometer (MISR) [8,18–20]. For AOD monitoring, ground-based passive aerosol monitoring networks and passive satellite sensor monitoring is more mature, and various algorithms have been developed for AOD monitoring based on passive sensors, such as Dark target and Deep Blue [5]. Passive sensors also play a key role in the monitoring of aerosol types. The information obtained from OMI regarding the absorbing aerosol index (UVAI), and the single scattering albedo (SSA), as well as the Angstrom index obtained by VIIRS can effectively assess the size, shape, and absorbing properties of aerosol particles [21,22]. However, passive sensors can only perform simple classification of aerosols by their size based on the different optical properties of aerosols and cannot obtain information on their vertical distribution. Bibi et al. [23] determined the types of absorbing aerosols by fine mode fraction, Angstrom exponent (AE), SSA as well as UVAI and studied the seasonal variation of aerosol types, confirming the feasibility of aerosol classification by CALIPSO data. Sabetghadam et al. [24] used the AOD and AE values obtained from MODIS to classify aerosols, and the results showed that the Mid-Eastern region of China is dominated by mixed aerosols throughout the year. Aerosol types in Nanjing, an urban-industrial city in the YRD region of eastern China, were also studied using MODIS with OMI between 2004–2015 [25]. In 2022, the aerosol generic classification using a novel satellite remote sensing approach (AEROSA) method was developed by Bilal et al. to classify aerosols using AOD versus AE to provide information on the number and size of aerosols, and it was found that AEROSA not only provided nine generic aerosol categories for all observations, but also adapted to changes in location and season, whereas general approach study aerosol types do not [26]. Lidar has the advantage of providing aerosol vertical distribution information and detailed classification of aerosols. The Cloud-Aerosol Lidar and Infrared Pathfinder Satellite Observations (CALIPSO) satellite, jointly developed by National Aeronautics and Space Administration (NASA) of the USA and National Center for Space Studies (CNES) of France, was launched in June 2006 in a sun-synchronous orbit with an orbital inclination of 98.2° and an altitude of 705 km above the ground. The CALIPSO satellite carries three main

detectors: Cloud-Aerosol Lidar with Orthogonal Polarization (CALIOP), Infrared Imaging Radiometer (IIR), and Wide Field Camera (WFC) [27]. The CALIOP is a dual-wavelength polarization lidar [11]. It is the most successful satellite-based atmospheric sounding lidar satellite, with the longest stable operation in orbit and the most mature development, which can provide continuous observation of the vertical distribution of aerosols on a global scale and distinguish typical aerosol types [28]. Consequently, it is a useful tool for studying aerosols in three dimensions.

Horizontal and vertical aerosol distribution characteristics at both regional- and global-scale, have been studied by domestic and international scholars using CALIPSO L3 data. For example, at the global scale, Pan et al. [29] investigated the temporal and vertical distribution characteristics of the optical properties of different aerosols in 2007–2019, and concluded that the seasonal distribution of global mean AOD for all types on land was in the order of summer (JJA) > spring (MAM) > autumn(DJF) > winter(SON) Mehta et al. [30] The trend changes of the main types of AOD showed that both dust and polluted dust AOD showed a decreasing trend unlike elevated smoke aerosols from 2006 to 2016. On a regional scale, Yang et al. [31] studied the aerosol properties of the Arctic, Antarctic, and Tibet Plateau from 2006 to 2019. The results showed that the AOD has obvious spatial and seasonal variation in these regions, with relatively large aerosol concentrations over Eurasia, the Ross Sea, and South Asia. Furthermore, Lu et al. [32] analyzed aerosol types and their vertical structure over East Asia, establishing that long-range transport of dust, pollution dust and smoke contributed significantly to the aerosol load over this region. Specific regions of China have also been studied. For example, based on the Weather Research and Forecasting Model with Coupled Chemistry (WRF-Chem) system Chen et al. [33] compared the dust emission, transport and deposition characteristics of the Taklamakan Desert (TD) and Gobi Desert in different seasons in East Asia from 2007 to 2011 to explore the contribution of the TD and Gobi Desert to dust concentration in East Asia. They found that 35% and 31% of dust from the Gobi Desert flowed to remote areas in East Asia, while only 25% and 23% of TD Dust was transported to remote areas in East Asia in MAM and JJA, respectively. The extent of dust aerosol presence in the vertical direction was also demonstrated: during MAM, 87% of dust extinction coefficient was concentrated at 1–4 km above the surface and only 8.1% at 4–6 km over the Gobi Desert; meanwhile TD transport is mainly at 4–10 km above the surface rather than 0–4 km downwind and more specifically at 4–6 km [34]. The high AOD of the North China Plain (NCP) is not only related to its own geographical factors and anthropogenic discharge, but also the sea ice and sea surface temperature in different ocean basins which affects the dust activity on the NCP [35]. The Yangtze River Delta(YRD) AOD is relatively high throughout the year, and anthropogenic aerosols are very evident [36]. Moreover, YRD MAM aerosols are more influenced by NCP dust, while JJA AOD is high due to aerosol hygroscopic growth, secondary aerosol formation, and agricultural biomass burning in the surrounding area [37]. However, although there have been many studies on regional aerosols in China, there are few comprehensive studies on 3D aerosol information over a long time period, using lidar data for the key regions in northern China and the YRD region. The TD and parts of the North Central Region of China (NCR) are the main sources of dust in China, and they are also important sources of dust for Central Asia. Meanwhile, the NCR is also impacted by TD dust. The TD, the NCR and the NCP constitute important pollution areas in northern China, and these areas are sensitive to climate change, which not only affects local climate, but also other regions of the world. Consequently, we considered these four regions important for aerosol characterization in a study.

The NCP and the YRD are the two most populated and economically developed regions in China. These areas have a large number of urban agglomerations and release a large amount of aerosol particles due to the large population, rapid economic development, and frequent human activities. The YRD is flat and unobstructed by topography and is consequently significantly affected by long-range transport of pollutants.

Therefore, the pollutant transport from NCP to YRD through the cold front channel is also considered as an important haze formation mechanism in YRD. Studies have shown that the PM_{2.5} contribution from NCP to YRD can be up to 31.5% of the total PM_{2.5} observed in YRD under some climatic conditions [38], therefore the integrated analysis of TD, NCR, NCP, and YRD is important for understanding the aerosol in these areas.

Previous studies on regional aerosols in China mostly concentrated on a single aerosol type or were limited to a single aerosol property. With the rapid economic and social development in China, atmospheric pollution is becoming increasingly serious, especially when considering a long timescale, and the impact of Chinese pollution control policies on aerosols has not been well analyzed. Consequently, it is necessary to integrate information on aerosols in the different regions and to evaluate the spatial and temporal distribution characteristics of regional aerosols by aerosol categories. Moreover, most of the previous studies are single-point analyses, or the information from individual stations was used to represent the situation of a region. Passive satellite remote sensing can observe aerosols on a large scale, but it is difficult to obtain information on their vertical distribution. In this paper, we analyze the AOD spatial and temporal distribution characteristics of the TD, NCP, NCR and YRD in Section 3.1 [39]. The vertical distribution of the aerosol extinction coefficient is discussed in Section 3.2 and the annual-average distribution of aerosol types in Section 3.3. Furthermore, we analyzed the impact of pollution control policies developed in China in 2013 versus 2018 on aerosol properties in the study area in Section 4.1 and the longitudinal variation of aerosol properties in the study area in Section 4.2.

2. Materials and Methods

2.1. Study Area

The TD (35–43° N, 75.5–90.5° E) is located in the Tarim Basin a large, closed mountain basin, surrounded by high mountains on all sides, and is the largest natural source of sand and dust emissions in China. Subsequent to sand and dust days, the dust is transported over long distances driven by cold, high pressure, and other air currents. The NCR (33–43° N, 90.5–110.5° E) includes most of the Gansu, Qinghai, and Shaanxi Provinces, which is a relatively harsh environment with overall poor vegetation cover and a large number of deserts. The NCP (33–43° N, 110.5–120.5° E) is the second largest plain in China, and is flat and open, with an average elevation of 50 m or less and many rivers, making it a typical alluvial plain. Studies have shown that the environmental quality of NCP has not been favorable because of its economic development and geographic factors, and its air quality continues to be poor [40,41]. The YRD (29–33° N, 116.5–122.5° E) is the primary economic zone in China, mainly located on the Taihu Lake Plain, in the lower reaches of the Yangtze River in China. The average temperature of the region is above 0 °C, which is typical subtropical monsoon climate. Externally transmitted pollutants along with local economic development and other anthropogenic activities have a large impact on air quality in the area [38] (Figure 1).

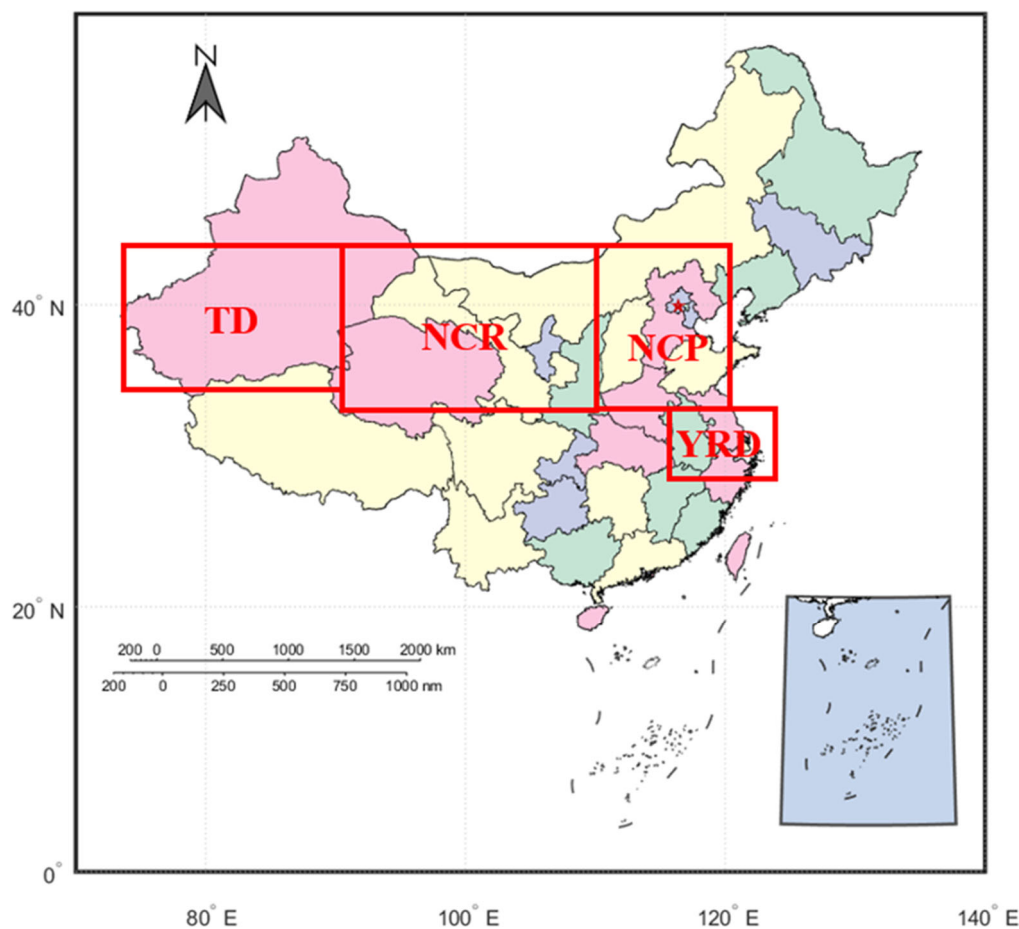


Figure 1. Study area. Red boxes indicate selected grids in the Taklamakan Desert (TD), Northern Central Region (NCR), North China Plain (NCP), and Yangtze River Delta (YRD).

2.2. Staellite Data

We chose the CALIOP Level 3 tropospheric aerosol profile product CAL_LID_L3_tropospheric_APro_CloudFree-Standard-V4 to study typical pollution transport regions in China, using mainly AOD, extinction coefficient, and aerosol types as parameters. The extinction characteristic inversion based on CALIPSO is mainly divided into three steps. First, the hierarchical features in the 532 nm attenuated backscattered signal are identified using Selective Iterative Boundary Locator; second, the hierarchical types are distinguished using Scene Classification Algorithms and three-pass data; finally, the extinction characteristics of the particles are obtained using Hybrid Extinction Retrievals Algorithm. Furthermore, CALIPSO can retrieve the aerosol type using information such as the laser-detected declination ratio, backscatter coefficient, subsurface type, and aerosol height [28]. The product provides all AOD (Columnar AODs), extinction coefficient, and AOD and extinction coefficient for the three main types of aerosols: Dust, elevated smoke, and polluted dust, as well as seven other aerosol types: clean marine, dust, polluted continental/smoke, clean continental, polluted dust, elevated smoke, and dusty marine. Level 3 aerosol profile extinction samples are filtered for quality [27], and have a high degree of accuracy. The highest quality data is obtained under cloud-free conditions compared to other air conditions, as the extinction inversion is minimized by the error of excessive cloud attenuation [28]. Therefore, cloud-free day- and nighttime data were used in this study. Among them, the all AOD obtained by CALIPSO has been validated in China based on AERONET measurement stations [39,42]. The temporal resolution of CALIPSO Level 3 data products is 1 month, with a spatial resolution of $2^\circ \times 5^\circ$, the vertical resolution is 60 m, and the detection altitude range is from sea level to 12.1 km, totaling

208 layers. As a polar-orbiting satellite, CALIPSO has long observation intervals and large orbital intervals, and cannot obtain continuous observations of the same area, which may miss brief and local pollution activities, though the Level 3 long time series monthly data products can compensate this shortcoming to some extent [43]. It should be noted that CALIPSO data were not available for February 2016, therefore this study does not include February 2016.

In order to further analyze the all AOD distribution of CALIPSO, and find out whether the AOD distribution of sensors based on different algorithms and models is consistent, we selected MODIS Level-3 grid product MOD08_D3 from January 2007 to December 2020, and the dataset used was 'AOD_550_Dark_Target_Deep_Blue_Combined_Mean' [44]. This AOD data was filtered from 10 km resolution level 2 daily products with QA = 3 and has been validated in the China region [9,45,46]. We also used the OMI AOD dataset 'FinalAerosolOpticalDepth500' from OMI near ultraviolet algorithm product. The spatial resolution of MODIS and OMI products is $1^\circ \times 1^\circ$, and the time resolution is 1 day [47]. The OMAERUVd product is produced with all data pixels that fall in a grid box with a quality filter and then averaged based on the pixel level OMI Level-2 aerosol data product OMAERUV. Similarly, OMAERUV dataset has been extensively validated in the Chinese region [6,48].

2.3. Data Processing

The CALIPSO satellite has a large spatial and temporal resolution. Consequently, we interpolated CALIPSO data into a $1^\circ \times 1^\circ$ grid. Only grid points with a proportion of observations greater than 2% during the study time were included in the AOD calculation when plotting the distribution of AOD, in order to avoid the influence of outliers and vacant values on the distribution of the mean AOD. When calculating the vertical distribution of the aerosol extinction coefficient in each layer, we defined the data(x) above three times the standard deviation of the mean value of each layer data and those below three times the standard deviation(δ) of the mean value(\bar{x}) as outliers to remove them [31].

$$x < \bar{x} - 3\delta \text{ or } x > \bar{x} + 3\delta \quad (1)$$

In order to avoid the impact of cloud pollution on the calculation results of UVAI and SSA, we eliminated the data with a cloud amount greater than 20% [49].

3. Results

3.1. Temporal and Spatial Distribution of AOD

The spatial distribution of the 14-year average cylindrical AOD according to CALIOP, MODIS and OMI in MAM, JJA, SON and DJF in China was retrieved (Figure 2). The all AOD values observed by different sensors show an inconsistent spatial pattern, especially those estimated by OMI and MODIS. However, CALIPSO has better coverage of all AOD inversion than MODIS and OMI. For example, for the bright surface of northern Mongolia, Qinghai-Tibet Plateau, and parts of Southeast Asia in winter, MODIS and OMI data may be absent due to high surface reflectivity and sensor algorithm [50]. However, the long-term observation of CALIPSO can show the all AOD distribution characteristics of these regions well. It is worth noting that areas in which OMI cannot effectively monitor all AOD throughout the year are mainly located where these values are low, and all AOD values retrieved by OMI are high in low-value areas compared to the values obtained from CALIPSO and MODIS (such as in Mongolia). Whether all AOD inversion of OMI will be greatly affected when all AOD values are low requires further investigation.

The high annual all AOD values in China are mainly located in the NCP, and in this region and Central China, the spatial distribution of MODIS and CALIPSO is more consistent. The complexity of aerosol types in the NCP and Central China, causes the OMI difficulties in data retrieval. Consequently, OMI may underestimate the all AOD values of the NCP and Central China [51]. However, in the TD, the seasonal mean change trend

of CALIPSO and OMI is more consistent. Compared with CALIPSO and OMI, MODIS shows a lower aerosol load in SON and DJF in the TD. Furthermore, TD all AOD changes obviously in different seasons, reaching the maximum in spring, and then decreasing gradually in JJA, SON and DJF. The dust aerosol generated in TD is then transported over long distances to other regions, impacting the atmospheric environment in other regions and contributing to global climate change.

The seasonal variation of the AOD in NCR is different from that of the TD. In the NCR, all AOD retrieved by OMI is significantly different from that observed by CALIPSO and MODIS, especially in the east of NCR where the all AOD of OMI is high. In contrast, in the eastern part of the NCR, OMI all AOD values are higher than MODIS and CALIPSO, which may be due to three main reasons [6]: (1) the larger OMI pixels, which are often contaminated by clouds; (2) the assumption of aerosol profiles; (3) the incorrect setting of surface reflectivity. In contrast, YRD shows a high all AOD value all year round, but the values given by different sensors vary. The most obvious area in China without OMI values is the Qinghai-Tibet Plateau, and the all AOD value of CALIPSO inversion in the Qinghai-Tibet Plateau is lower than the value noted by MODIS. An important reason for the underestimation of all AOD by CALIPSO may be its low signal-to-noise ratio. The ability of CALIPSO to detect weak aerosol layers is diminished and highly diffuse and thin aerosol layers below the CALIPSO detection threshold may be ignored. Moreover, the 16-day sampling frequency of CALIPSO may lead to missed pollution events [52].

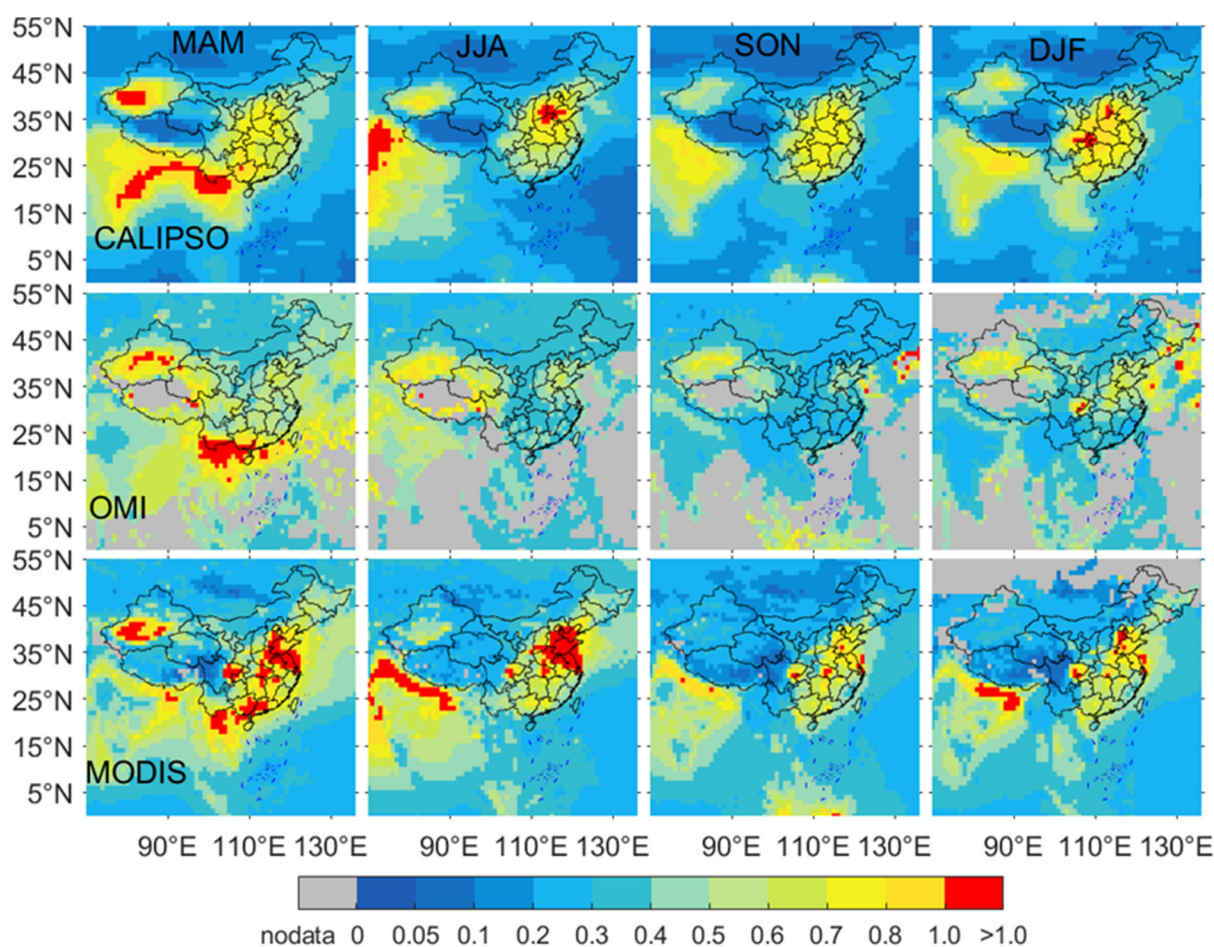


Figure 2. Spatial distribution of seasonal average all aerosol optical depth (AOD) for CALIPSO 532 nm, OMI 500 nm, and MODIS 550 nm in the Chinese region from 2007 to 2020. The horizontal axes represent CALIPSO, OMI, and MODIS sensors, respectively, and the vertical coordinates represent spring, summer, autumn, and winter, respectively.

The distribution of different types of AOD have obvious seasonal variations (Figure 3). The values for TD dust AOD is the highest, and the dust AOD value in this region is higher than those of elevated smoke- and polluted dust AOD in different seasons. The AOD values of TD dust are the highest in spring and declined thereafter (Table 1). However, the NCR AOD values did not show this decline in autumn and winter. The seasonal distribution of the main types of AOD in China show that the TD and NCR have significant dust aerosol diffusion in MAM. This may be the reason for the higher dust AOD in the NCP and YRD during MAM when compared to other seasons. The primary areas where elevated smoke AOD is high are in northern Yunnan and Guangxi in spring. This is because under the influence of some parts of Southeast Asia, the elevated smoke AOD is higher in northern Yunnan and Guangxi regions of China during MAM. The large amount of biomass activities in Southeast Asia produces smoke aerosols, and then the long-distance transmission of these affect the climate in the downwind region [53,54]. The second highest incidence of elevated smoke AOD is in Central China, NCP and YRD, during the summer. The annual elevated smoke aerosol distribution of TD and NCR is not obvious, with an elevated smoke AOD value between 0–0.05. The presence of higher elevated smoke AOD in the NCP and YRD during JJA is significantly related to industrial emissions, secondary aerosol formation, and biomass burning during harvest season in both regions [37]. The annual concentration of polluted dust aerosol in the NCP is higher than that observed in other regions in China. During JJA, the AOD values of different types of aerosol are generally higher in the NCP. This is mainly due to three reasons: (1) higher temperature and humidity, which is conducive to the air-particle conversion of organic aerosols and aerosol particle hygroscopic growth, which leads to an increase in AOD [55]. (2) Industries in the area are growing rapidly and the emissions of a large amount of pollutants leads to an increase in AOD. (3) JJA is crop harvesting season, and anthropogenic biomass burning increases AOD [56]. Meanwhile, studies show that the increase of secondary aerosols is one of the principal factors for the formation of haze during JJA, SON and DJF in North China [56,57]. Polluted dust aerosols observed in DJF are larger and the influence range is shifted to the southeast, probably due to the transit of cold fronts and local emissions [58]. The spatial distribution of polluted dust aerosol is centered on the NCP, and decreases irregularly with the increase of distance from NCP. The high concentration of polluted dust aerosols may be related to human activities, special topography, meteorological conditions, and transmission from external regions to this area [59]. In DJF, the concentration of polluted dust aerosol is the highest in NCP with the largest range, and the high incidence of polluted dust AOD shifts to the southeast. The correlation between polluted dust aerosol distribution and dust aerosol distribution in China is low, which may be mainly due to the origins of polluted dust, with less anthropogenic activities in the dust emission source area, while polluted dust is generated during the transmission of dust from one area to another or mixed with local anthropogenic aerosols to generate polluted dust aerosol after transmission to other areas (Figure 3).

Table 1. Seasonal mean values of optical thickness of ALL, Dust, ES and Polluted Dust aerosol in TD, NCR, NCP and YRD from 2007 to 2020.

| Region Type | TD | | | | NCR | | | | NCP | | | | YRD | | | |
|-----------------------|----------------------|-------|-------|----------------------|------------------------|-------|-------|-------|-----------------------|-------|-------|-------|-------------------|-------|-------|-------|
| | MAM | JJA | SON | DJF | MAM | JJA | SON | DJF | MAM | JJA | SON | DJF | MAM | JJA | SON | DJF |
| all | 0.543 | 0.400 | 0.292 | 0.287 | 0.331 | 0.269 | 0.206 | 0.234 | 0.495 | 0.590 | 0.428 | 0.464 | 0.570 | 0.508 | 0.489 | 0.529 |
| dust | 0.513 | 0.343 | 0.242 | 0.164 | 0.234 | 0.096 | 0.072 | 0.086 | 0.170 | 0.027 | 0.038 | 0.057 | 0.113 | 0.005 | 0.019 | 0.042 |
| | (94.4% 85% 83% 57%) | | | | (71% 36% 35% 37%) | | | | (34% 4.6% 8.9% 12%) | | | | (20% 1% 4% 8%) | | | |
| elevated smoke | 9.6×10^{-4} | 0.004 | 0.001 | 6.3×10^{-4} | 0.004 | 0.024 | 0.007 | 0.002 | 0.014 | 0.102 | 0.022 | 0.015 | 0.057 | 0.145 | 0.060 | 0.044 |
| | (0.2% 1% 0.3% 0.2%) | | | | (1.2% 9% 3.4% 0.9%) | | | | (3% 17% 5% 3%) | | | | (10% 29% 12% 8%) | | | |
| polluted dust | 0.025 | 0.045 | 0.042 | 0.0905 | 0.081 | 0.098 | 0.093 | 0.120 | 0.243 | 0.209 | 0.236 | 0.294 | 0.253 | 0.090 | 0.134 | 0.235 |
| | (4.6% 11% 14% 32%) | | | | (24% 36% 45% 51%) | | | | (49% 35% 55% 63%) | | | | (44% 18% 27% 44%) | | | |
| others | (0.8% 3% 2.7% 10.8%) | | | | (3.8% 19% 16.6% 11.1%) | | | | (14% 43.4% 31.1% 22%) | | | | (26% 52% 57% 40%) | | | |

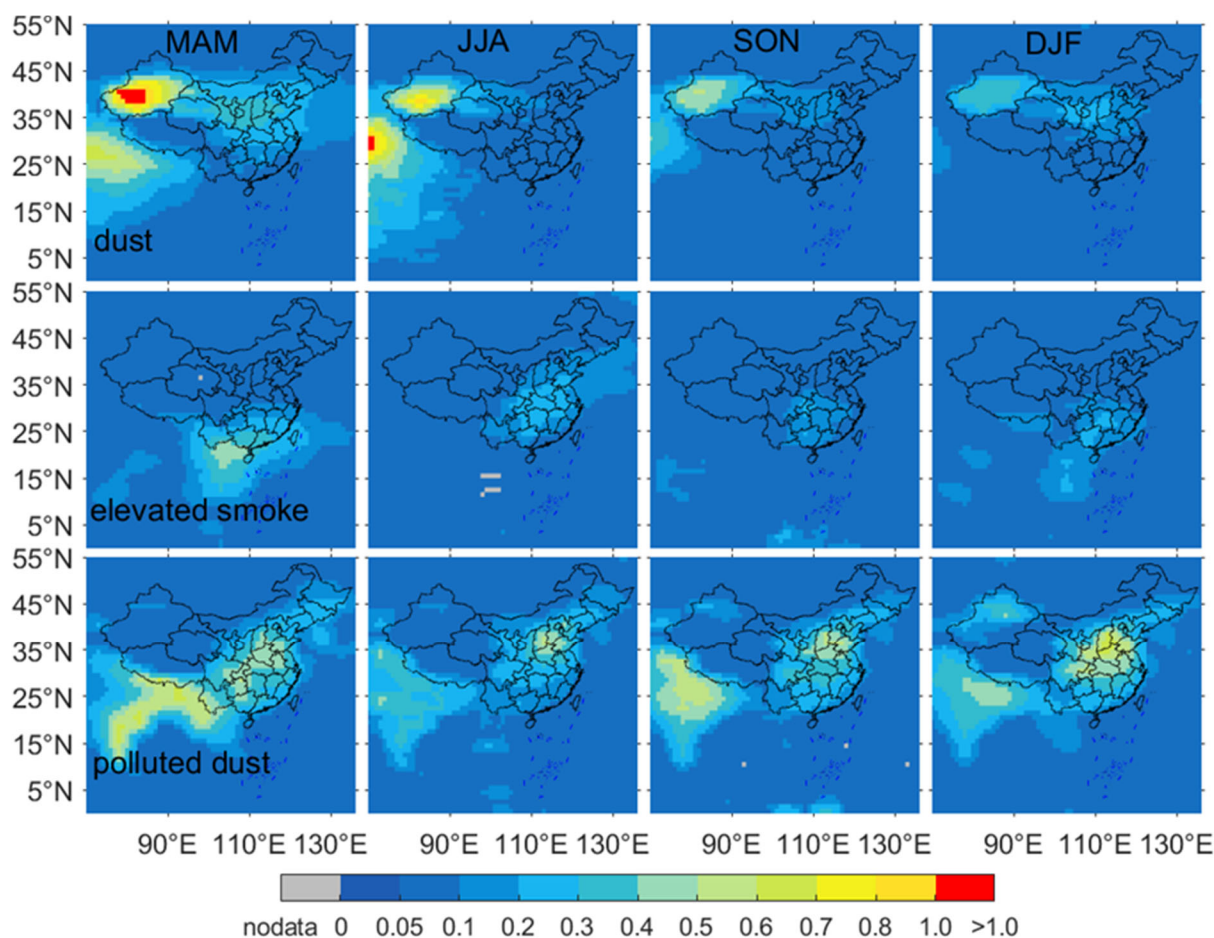


Figure 3. Average aerosol optical depth (AOD) distribution of dust, polluted dust, elevated smoke over China from 2007–2020 based on CALIPSO data. Rows represent aerosol types (dust, polluted dust, elevated smoke), columns represent seasons (MAM, JJA, SON, DJF).

3.2. Vertical Distribution of Aerosol Extinction Coefficient

The vertical distributions of the extinction coefficient in the TD, NCR, NCP, and YRD regions differ substantially (Figure 4), and are mainly distributed below 8 km (Table 2). In general, the all AOD extinction coefficient of NCP and YRD have a wider vertical distribution at 0–12 km compared to TD and NCR, and the seasonal variation of all extinction coefficient is also weaker in NCP and YRD compared to TD and NCR. The dominant aerosol type varies from season to season at different elevations in the regions, except for TD, where the dominant aerosol type is dust throughout the year,

The main aerosol type in TD at different altitudes is dust, especially in MAM, JJA and SON, where the extinction coefficient value of dust is close to the all-extinction coefficient value. In DJF, the 4–6 km extinction coefficient range decreases significantly, and in addition to dust aerosols, the contribution of polluted dust is also larger at 0.8–4 km. The seasonal variation of extinction coefficient in NCR is very obvious, and during MAM, the distribution patterns of all-, dust- and polluted dust extinction coefficients are basically the same, while during JJA, elevated smoke aerosols also start to appear, and the aerosol types are more complex. Below 2.8 km in the NCR during JJA, SON and DJF, polluted dust aerosol extinction coefficient values are larger than that of dust aerosol, while above 2.8 km they show different patterns. For instance, the amounts of dust aerosol are larger than polluted dust aerosol during JJA, while polluted dust and dust extinction coefficients are more similar during SON. During DJF, dust aerosol makes a larger contribution than polluted dust aerosol above 3 km. Unlike for TD and NCR, all extinction coefficient peaks for NCP and YRD are closer to the ground, the extinction coefficient layer is mainly

concentrated under 4 km, and the contribution of polluted dust aerosol is obvious throughout the year. We found that high values of extinction coefficient are mainly located in NCP and YRD, while NCP DJF polluted dust extinction coefficient is the largest, mainly because DJF coal-fired heating emits a large amount of aerosol particles, accompanied by a strong inversion temperature and stable atmospheric boundary layer in DJF which impedes diffusion of pollutants [58]. In MAM and DJF, NCP and YRD dust extinction coefficients are higher in the 0–2 km zone, and the values observed during MAM is higher than those noted during DJF, which is correlated with dust transport in the NCR under certain meteorological conditions [38]. Elevated smoke aerosols in JJA over the NCP surpasses polluted dust aerosols above 2 km, while in the YRD elevated smoke aerosols are already obvious near the surface and appear higher than polluted dust. It is worth noting that although the YRD elevated smoke aerosol extinction coefficient is significantly weakened in SON, the elevated smoke aerosol extinction coefficient is still larger than that of polluted dust at 2 km overhead.

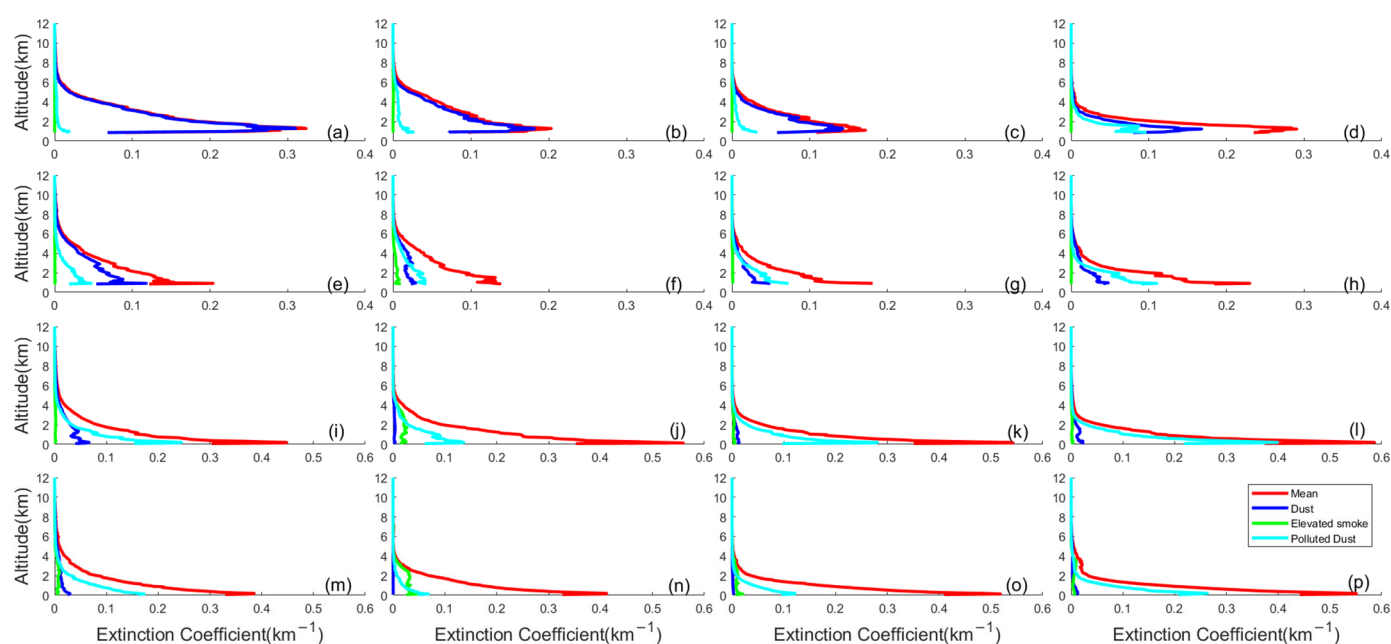


Figure 4. Seasonal vertical distribution of average extinction coefficient (red solid line), dust extinction coefficient (blue solid line), Elevated smoke extinction coefficient (green solid line), and polluted dust extinction coefficient (cyan solid line) for TD (a–d), NCR (e–h), NCP (i–l), and YRD (m–p) from 2007 to 2020.

Table 2. Vertical mean values of extinction coefficients of all, dust, elevated smoke and polluted dust aerosols in TD, NCR, NCP and YRD regions from 2007 to 2020.

| Region | EC | EC_Dust | EC_Elevated_Smoke | EC_Polluted_Dust |
|--------|----------------|----------------|-------------------------------|------------------------------|
| TD | 0–2 km: 0.2190 | 0–2 km: 0.1829 | 0–2 km: 1.27×10^{-4} | 0–2 km: 0.0297 |
| | 2–4 km: 0.0784 | 2–4 km: 0.0692 | 2–4 km: 3.22×10^{-4} | 2–4 km: 0.0076 |
| | 4–6 km: 0.0193 | 4–6 km: 0.0153 | 4–6 km: 3.05×10^{-4} | 4–6 km: 0.0033 |
| | 6–8 km: 0.0028 | 6–8 km: 0.0018 | 6–8 km: 1.17×10^{-4} | 6–8 km: 8×10^{-4} |
| NCR | 0–2 km: 0.1368 | 0–2 km: 0.0535 | 0–2 km: 0.0042 | 0–2 km: 0.0565 |
| | 2–4 km: 0.0525 | 2–4 km: 0.0280 | 2–4 km: 0.0021 | 2–4 km: 0.0182 |
| | 4–6 km: 0.0169 | 4–6 km: 0.0117 | 4–6 km: 5.68×10^{-4} | 4–6 km: 0.0042 |
| | 6–8 km: 0.0034 | 6–8 km: 0.0024 | 6–8 km: 1.52×10^{-4} | 6–8 km: 8×10^{-4} |
| NCP | 0–2 km: 0.2181 | 0–2 km: 0.0258 | 0–2 km: 0.0113 | 0–2 km: 0.1109 |
| | 2–4 km: 0.0378 | 2–4 km: 0.0096 | 2–4 km: 0.0080 | 2–4 km: 0.0153 |
| | 4–6 km: 0.0070 | 4–6 km: 0.0031 | 4–6 km: 0.0013 | 4–6 km: 0.0024 |
| | 6–8 km: 0.0018 | 6–8 km: 0.0011 | 6–8 km: 1.53×10^{-4} | 6–8 km: 5.2×10^{-4} |
| YRD | 0–2 km: 0.2218 | 0–2 km: 0.0131 | 0–2 km: 0.0212 | 0–2 km: 0.0798 |
| | 2–4 km: 0.0325 | 2–4 km: 0.0055 | 2–4 km: 0.0138 | 2–4 km: 0.0093 |
| | 4–6 km: 0.0066 | 4–6 km: 0.0030 | 4–6 km: 0.0017 | 4–6 km: 0.0018 |
| | 6–8 km: 0.0022 | 6–8 km: 0.0011 | 6–8 km: 7.3×10^{-4} | 6–8 km: 4.1×10^{-4} |

3.3. Spatial and Temporal Distribution of Aerosol Types

To further understand the spatial and temporal distribution of aerosol types in the study area, we investigated the average aerosol type occurrence frequency (OF) in the Chinese region from 2007 to 2020 (Figure 5). CALIPSO classifies aerosol types in the troposphere into seven subtypes by the scene classification algorithm [60]. The algorithm uses comprehensive attenuation backscattering and particle depolarization measurement, surface type, layer top and foundation height to identify aerosol subtypes. Where i–vii represent respectively clean marine, dust, polluted continental/smoke, clean continental, polluted dust, elevated smoke, and dusty marine. On the whole, the OF distribution of aerosol types in different regions has obvious differences. Clean- and dusty marine aerosols are mainly concentrated in the eastern part of China and decrease until they disappear further inland. Clean continental aerosols are mainly encountered in land areas, and the overall OF is low, with the lowest OF in the TD and NCR regions. The largest OF of dust aerosols is in the Qinghai region of TD and NCR, which then gradually decreased to the east. The overall dust aerosol levels in northern China are higher than those in southern China [53,54]. Notably, polluted continental/smoke aerosol levels are higher in southern than in northern China. Furthermore, from the OF distribution of polluted continental/smoke, it can be surmised that the high OF observed in the NCP and Northeast China may be influenced more by conditions in other countries. Polluted dust aerosol for TD is at a lower level in the study area, while levels observed in NCP and YRD are higher, which is consistent with the conclusion in 3.1. Elevated smoke aerosols are mainly distributed in the northeast and southeast regions of China.

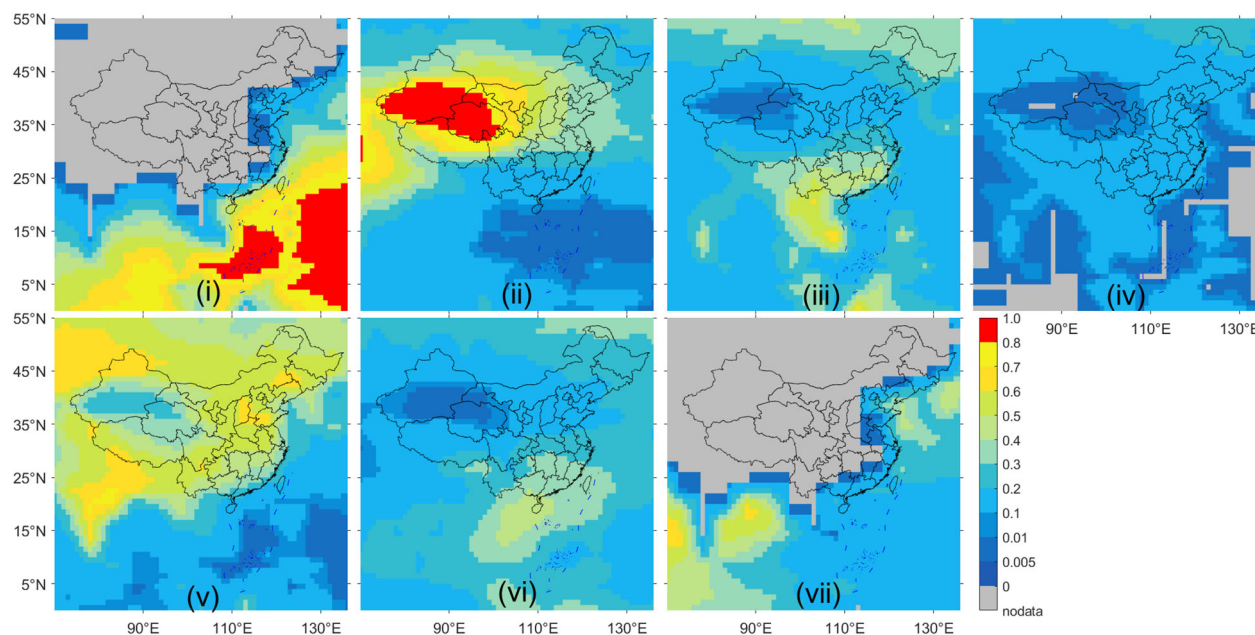


Figure 5. Multi-year average OF of seven aerosol types in China from 2007 to 2020. The numbers (i–vii) represent clean marine, dust, polluted continental/smoke, clean continental, polluted dust, elevated smoke, and dusty marine, respectively.

In TD, dust is the most common aerosol, followed by polluted dust. The OF changes obviously throughout the seasons, with polluted dust OF being the highest during DJF, reaching 39.5% (Table 3). Elevated smoke aerosol OF in TD is the highest during summer (OF = 1.2%), while other types of aerosols are not obvious, and the OF is less than 1%. The dust- and polluted dust aerosol OF observed in NCR are the highest, but their seasonal variation is different from that recorded for TD. The dust aerosol OF in NCR during JJA is the lowest, while the polluted dust aerosol OF increased from MAM to JJA. Subsequently, the polluted dust aerosol OF during JJA, SON and DJF in NCR is higher than 0.4. Clean- and dusty marine aerosols are only found in some areas of NCP and YRD. Clean marine aerosols in these two areas first increase and then decrease (values recorded during JJA reaches the maximum), while dusty marine aerosol's seasonal variation trend is the opposite of that observed for clean marine. There are many types of aerosols present in NCP and there are some variations over the seasons. On the NCP, polluted dust aerosol is the most obvious over the entire year, while elevated smoke aerosol has the second highest OF in JJA, and dust aerosol has the second highest OF in SON and DJF. The trends of NCP polluted continental/smoke, clean continental and elevated smoke aerosols are the same, and they all decrease after the highest JJA value. Furthermore, YRD aerosol levels show great variation throughout the seasons, dust and polluted dust aerosol are dominant in MAM, while the polluted continental/smoke and elevated smoke OF of JJA is higher, and polluted dust is the most obvious aerosol type in SON and DJF. The large variation in the dominant aerosol type OF in YRD in different seasons is due to the influence of a high-pressure field in the northern parts in DJF. During MAM, dust from NCR to YRD is transported with high wind from north to south, this has also been reported to be the case in SON [61,62]. During JJA, frequent industrial activities and biomass burning are important causes of YRD polluted continental/smoke and elevated smoke aerosol concentrations [63].

After analyzing the aerosol types in the study area, we observed that, TD, NCR, NCP and YRD showed a pattern of aerosol type occurrence from west to east in different seasons. The OF of dust aerosol gradually decreases, while the OF of polluted continental/smoke aerosol gradually increases, but the OF of TD polluted continental/smoke aerosol is larger in DJF than it is in NCR; polluted dust aerosol increases from TD eastward

and decreases after the maximum value is reached in NCP. In TD, NCR, NCP, and YRD clean continental, elevated smoke aerosols are most obvious in JJA, while clean- and dusty marine aerosols only occur in some areas of NCP and YRD, and clean marine aerosols increase first and then decrease in both areas (reaching the maximum in JJA), while the seasonal trend of dusty marine aerosol OF is opposite to clean marine aerosols. This is mainly due to the prevailing southerly wind in the eastern part of China in JJA.

The regions with higher elevated smoke aerosol OF are located in northeast and southeast China. The higher elevated smoke aerosol OF in northeast China may be related to human activities during the heating period, which is generally from October to March of the following year in the northern China. The burning of fossil fuels in the heating period and the increase of vehicle exhaust emissions in the low temperature period will directly lead to the increase of elevated smoke aerosol. The higher levels of elevated smoke aerosol in southeast China may be caused by external transport. The polluted continental/smoke aerosols in southern China are present at higher levels than those in northern regions due to the influence of some regions in Southeast Asia [53,54].

Table 3. Seasonal Occurrence Frequency (OF) of seven aerosol types on TD, NCR, NCP, and YRD in 2007–2020.

| Region | Season | Aerosol Type | | | | | | |
|--------|--------|--------------|-------|----------------------------|-------------------|---------------|----------------|--------------|
| | | Clean Marine | Dust | Polluted Continental/Smoke | Clean Continental | Polluted Dust | Elevated Smoke | Dusty Marine |
| TD | Spring | 0 | 0.852 | 0.005 | 0.002 | 0.138 | 0.003 | 0 |
| | Summer | 0 | 0.712 | 0.009 | 0.006 | 0.261 | 0.012 | 0 |
| | Autumn | 0 | 0.761 | 0.008 | 0.004 | 0.223 | 0.005 | 0 |
| | Winter | 0 | 0.552 | 0.040 | 0.006 | 0.395 | 0.008 | 0 |
| NCR | Spring | 0 | 0.752 | 0.007 | 0.003 | 0.230 | 0.008 | 0 |
| | Summer | 0 | 0.464 | 0.046 | 0.010 | 0.436 | 0.045 | 0 |
| | Autumn | 0 | 0.536 | 0.031 | 0.007 | 0.412 | 0.015 | 0 |
| | Winter | 0 | 0.542 | 0.028 | 0.005 | 0.419 | 0.006 | 0 |
| NCP | Spring | 0.004 | 0.493 | 0.027 | 0.010 | 0.394 | 0.029 | 0.043 |
| | Summer | 0.027 | 0.128 | 0.158 | 0.037 | 0.425 | 0.200 | 0.024 |
| | Autumn | 0.020 | 0.214 | 0.091 | 0.019 | 0.530 | 0.057 | 0.069 |
| | Winter | 0.013 | 0.276 | 0.062 | 0.015 | 0.542 | 0.028 | 0.064 |
| YRD | Spring | 0.021 | 0.406 | 0.047 | 0.008 | 0.356 | 0.053 | 0.109 |
| | Summer | 0.166 | 0.048 | 0.256 | 0.040 | 0.177 | 0.295 | 0.018 |
| | Autumn | 0.143 | 0.101 | 0.209 | 0.024 | 0.287 | 0.152 | 0.083 |
| | Winter | 0.064 | 0.240 | 0.094 | 0.011 | 0.408 | 0.095 | 0.088 |

In order to test the aerosol types monitored by CALIPSO, we compared them to that of SSA and the average distribution UVAI from 2007 to 2020 (Figure 6). SSA is one of the most important parameters of aerosol optical properties, which is defined as the proportion of scattering extinction coefficient to all extinction coefficient. Aerosols that contribute more to SSA value are mainly sulfate and sea salt aerosol [64]. Furthermore, UVAI is a qualitative parameter of the degree of ultraviolet absorption of aerosol, which can reflect the existence and spatial distribution characteristics of absorptive aerosols. The UVAI values are positive when it is a regional absorption aerosol, and negative or close to zero when it is a scattering aerosol. Aerosols that contribute more to UVAI are mainly biomass burning such as, agricultural- and fossil fuel burning as well as dust. We can compare the aerosol types detected by CALIPSO based on these data [65]. The SSA based on OMI acquisition has been validated in the Chinese region, and the results show that the agreement between OMI and AERONET data is poor in areas that are more significantly

affected by human activities [66]. The global and regional use of OMI UVAI based on OMI has proved the reliability of UVAI [21,64].

The overall UVAI in China shows high values in the northwest and southeast while the other regions are relatively low (Figure 6). The most obvious areas where UVAI values are high and SSA values low were located in the TD, while the eastern part of the NCR also shows higher UVAI. Dust aerosol produced by the TD is a critical component of the absorbing aerosol and therefore causes the higher UVAI and lower SSA, which is consistent with the conclusion that dust aerosol dominates at this site as demonstrated by CALIPSO. Moreover, the high UVAI values in the eastern part of the NCR are to some extent indicative of dust aerosol transport. The second largest location where UVAI values are high area is located in the Sichuan basin and Guangxi in southwest China, where UVAI values were >1.2 and SSA values mainly lie between 0.8–0.9, proving that a mixture of black carbon and dust may dominate the aerosol in this area [23]. From the CALIPSO results, we can see that polluted dust, dust and polluted continental/smoke are all present in high proportions in the southwest, indicating that the results given by CALIPSO, and OMI are consistent. In the NCP and YRD, we observed UVAI values ranging from 0–2.0, and SSA values from 0.8–0.96 are present. This may be the result of the complex aerosol types due to frequent human activities and geography in these areas, and CALIPSO results corroborate this. There are seven aerosol types in the NCP and YRD, which are the most complex aerosol types in China.

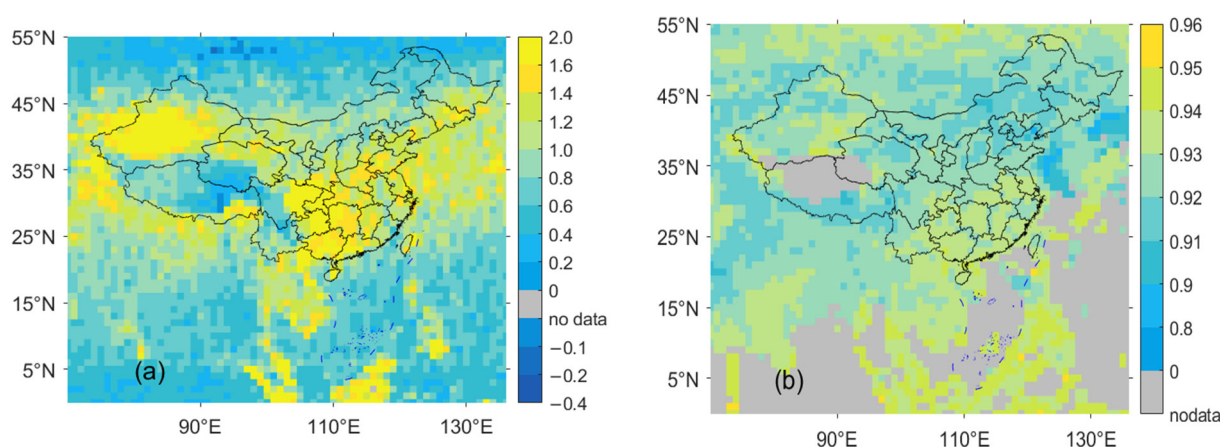


Figure 6. Spatial distribution of multi-year mean ultraviolet aerosol index (UVAI) and single scattering albedo (SSA) for 2007–2020 obtained based on the ozone monitoring instrument (OMI). (a): UVAI; (b): SSA.

4. Discussion

4.1. Effects of Chinese Pollution Control Policies on the Aerosol Properties of TD, NCR, NCP, and YRD

In 2012 and 2013, after a large area of smog appeared in Beijing-Tianjin-Hebei, YRD, and other cities, the problem of air pollution control came to the attention of the public and government departments. In 2013, China's State Council issued the "Action Plan for the Prevention and Control of Air Pollution", which formally established the air pollution prevention and control model with the concentration of atmospheric particulate matter as the core control target. The main points of the policy in 2013 were the requirements for provinces to effectively address the problem of particulate matter emission concentrations from coal combustion, dust, motor vehicle exhaust, restaurant fumes, and straw-burning pollution. After the implementation of the 2013 policy, the annual average PM_{2.5} concentrations in important cities across the country decreased by up to 35% in 2017 compared to 2013, with the annual average PM_{2.5} concentration in Beijing dropping from 90 $\mu\text{g}/\text{m}^3$

to $58 \mu\text{g}/\text{m}^3$. The fine particulate matter concentrations in the Beijing-Tianjin-Hebei, YRD and Pearl River Delta regions decreased by about 25%, 20% and 15%, respectively. To promote continuous improvement in air quality and achieve the “13th Five-Year Plan” air quality improvement target, the State Council issued the “Three-Year Action Plan for Winning the Blue Sky Defense War” in 2018, which further consolidates and strengthens the control structure over PM_{2.5} and other typical compound air pollutants as the core. After three years of efforts, the national and key regional air quality should be significantly improved, and the national annual average PM_{2.5} concentration should decrease by 20% in 2020 compared to 2017; the three key regions of Beijing, Tianjin, Hebei and the surrounding areas, the YRD, and Fenwei Plain should show decreases by 21%, 26%, and 23% respectively [67–71]. Consequently, whether long-term pollution control policies have an effect on AOD, extinction coefficient at different altitudes, and aerosol types in the TD, NCR, NCP, and YRD regions were investigated in this section.

We plotted the multi-year monthly average changes of all, dust, elevated smoke, and polluted dust AOD values in the four study areas during 2007–2020. However, due to the lack of data in February 2016, there were data interruptions in 2016–2017. Seasonal variation of AOD varies greatly in different regions (Figure 7). From the change observed in all AOD values, we found that the all AOD of YRD fluctuates greatly over time, and the months with the maximum AOD value differs between years. The all AOD showed a downward trend in the four regions ($-0.03\% < \text{slope} < -0.18\%$), in which the downward trend of the YRD and NCP was more obvious (the slope of YRD fitting curve: -0.18% ; the slope of NCP fitting curve: -0.12%), which is significantly related to the implementation of stringent long-term emission control measures in these regions in China from 2013 and 2018 [38]. The all AOD values of NCP and YRD are higher than those of TD and NCR. Furthermore, the all AOD value for NCP in summer is the highest, with the average value being up to 0.59 in several years. Elevated smoke AOD values in the four study areas are the highest in summer (JJA) followed in decreasing order by autumn (SON), spring (MAM) and winter (DJF). The lower values of elevated smoke AOD present in the TD and NCR indicate that these two regions are influenced less by industrial development and human activities. The TD is sparsely populated, but elevated smoke AOD and polluted dust AOD have shown a slight upward trend over the years, indicating that the contribution of human activities to pollution in remote areas has begun to increase in recent years. Notably, NCR, NCP, YRD elevated smoke- and polluted dust AOD values show a downward trend from 2007 to 2020, but the elevated smoke AOD of YRD is still much higher than that of the other three regions. The higher elevated smoke AOD in YRD is due to the greater contribution of transportation, industry, and biomass burning in YRD to the regional elevated smoke AOD [72]. Kang et al. [37] showed through a backward trajectory model study that some of the YRD cities in the MAM would be influenced by dust in northern and northwestern China, leading to an increase in AOD in the region. A weak upward trend is observed for TD elevated smoke- and polluted dust AOD values from 2007 to 2020. The all- and dust AOD values of MAM TD and NCR are higher than those of other seasons in the entire year. Notably, in MAM, the monthly mean change of dust AOD in the four regions has a high consistency, while the local dust emission sources of NCP and YR are lower. Due to the intensification of MAM frontal activity and dry and windy weather, dust enters the atmosphere under the action of wind [34]. So the dust of TD and NCR will be transmitted to NCP and YRD, resulting in the high consistency of the MAM dust variation trend of TD, NCR, NCP, and YRD. According to the trend chart of polluted dust AOD changes over the years, NCP annual polluted dust AOD is generally higher than that of the other three regions. In DJF, the polluted dust AOD change trend of TD, NCR and NCP is highly consistent.

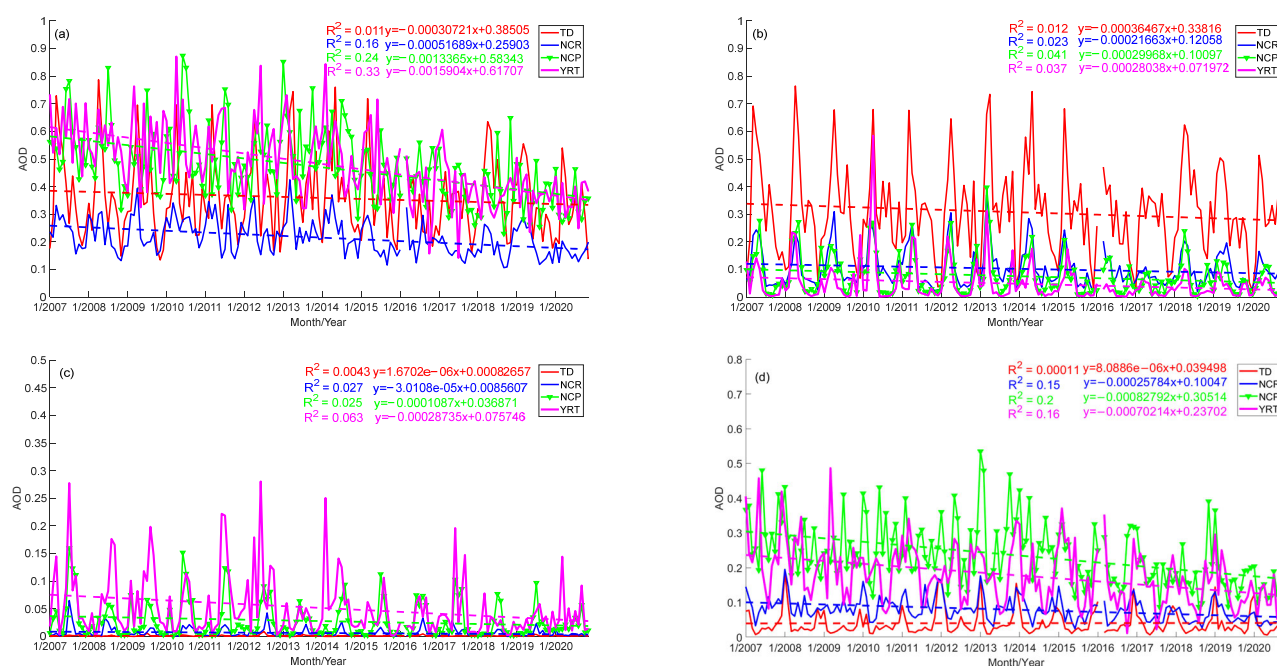


Figure 7. Temporal variation in monthly aerosol optical depth (AOD) anomalies from 2006 to 2020 over China. The dotted different colors represent the linear trends. The first behavior is (a): all AOD, (b): dust AOD; The second behavior (c): elevated smoke AOD, (d): polluted dust AOD.

The comparative analysis of the spatial distribution maps of the dominant types of AOD from 2007–2013, 2014–2018, and 2019–2020 shows that the spatial distribution characteristics of the AOD in the interval range of different years are similar, but there are substantial changes in the AOD data (Figure 8). First, both the NCP and YRD are obvious high value areas, and with the implementation of pollution prevention and control policies, the all AOD of the NCP and YRD decreased significantly in 2013–2018 and 2018–2020, and the high value all AOD decreased significantly, while the dust AOD basically did not change, so the main factor affecting the NCP and YRD air quality is polluted dust. All AOD changes in the NCP and YRD are more related to the contribution of the main aerosol type, polluted dust. Meanwhile, the YRD elevated smoke AOD has started to decrease gradually with the implementation of pollution policies, and by 2018–2020, the elevated smoke AOD above 0.05 in YRD has disappeared. The TD is dominated by dust aerosols, and the change of TD all AOD is not obvious because dust aerosols are less affected by human influence, which is also the reason for the smaller change in dust AOD distribution. This is also why the dust AOD distribution shows a low variation. However, from the dust distribution map of China, it can be seen that the AOD values in the dust transmission affected areas of TD and NCR have significantly weakened, which may be related to the afforestation and sand control in China [73]. The air quality changes in the eastern part of NCR are influenced by the urban agglomeration in the Guanzhong Plain, and the pollution prevention and control policies also make the optical thickness of polluted dust aerosols in this area significantly lower, which is also an important reason for the lower all AOD in this area.

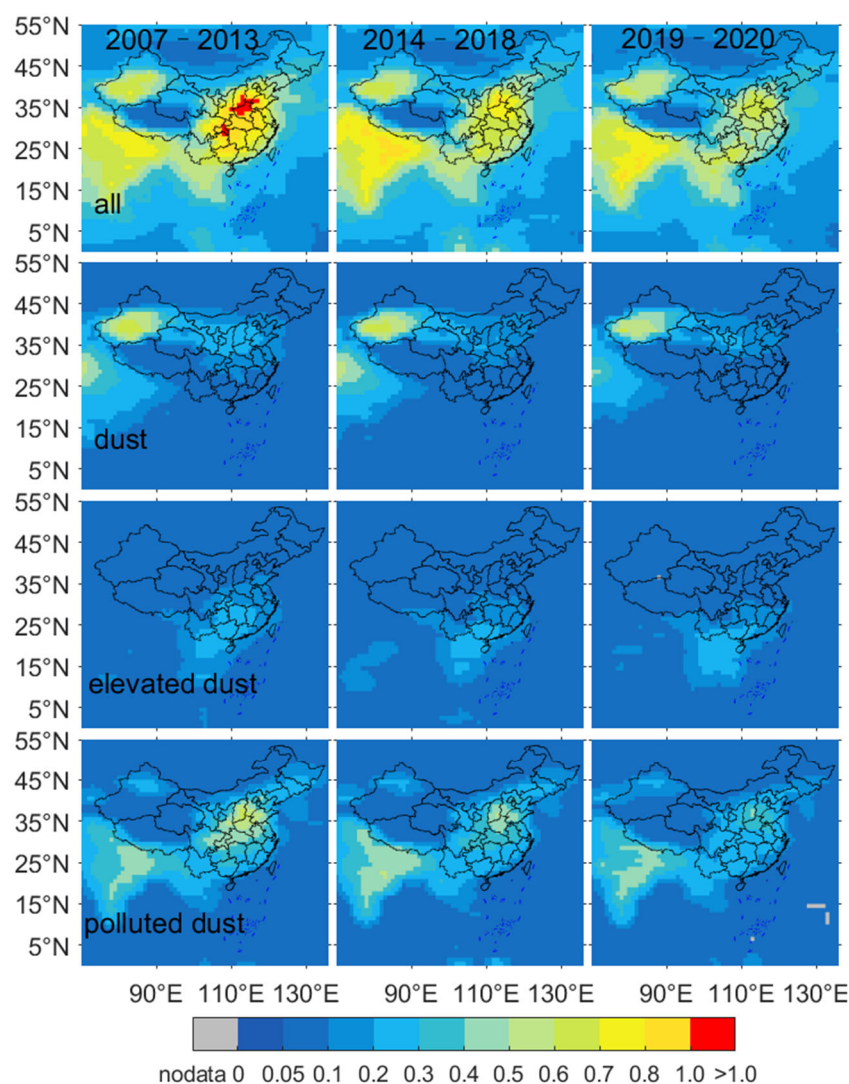


Figure 8. Spatial distribution of average aerosol optical depth (AOD) for the Taklimakan Desert (TD), North central region of China (NCR), North China Plain (NCP), and Yangtze River Delta (YRD) for 2007–2013, 2014–2018, and 2019–2020. The horizontal columns represent the types (all, dust, elevated smoke, polluted dust, in order) and the vertical columns represent the years (2007–2013, 2014–2018, 2019–2020, in order).

Changes in the dominant extinction coefficient profiles in the four regions, TD, NCR, NCP, and YRD were observed for the three time periods 2007–2013, 2014–2018, 2019–2020 (Figure 9). Overall, we found that the width of vertical distribution of TD, NCP, and YRD decreased per year, but this was not the case for NCR. The significant decrease in the dust extinction coefficient of TD in 2018–2020 may be mainly related to the 16-day sampling frequency period of CALIPSO, which may have led to some missed dust events. However, the longer time span of 2007–2018 should resolve this problem. The width of vertical distribution of NCR did not decrease in 2013–2018 mainly due to the larger polluted dust extinction coefficient near 1 km, but with the increase of height, the extinction coefficient was significantly smaller than that observed in 2007–2013. Consequently, the overall extinction coefficient is still decreasing. The decrease in the width of the vertical distribution of the all-extinction coefficient coefficients of NCP and YRD is also obviously related to the decrease of the polluted dust extinction coefficient, while the changes in elevated smoke and dust extinction coefficient are not obvious. In particular, the NCP and YRD, as important economic and population activity areas in China, are more responsive to

pollution prevention and control policies, with maximum values of 0.62, 0.47, and 0.38 for NCP near-surface extinction coefficient and 0.57, 0.41, and 0.34 for YRD in 2007–2013, 2014–2018, and 2019–2020, respectively.

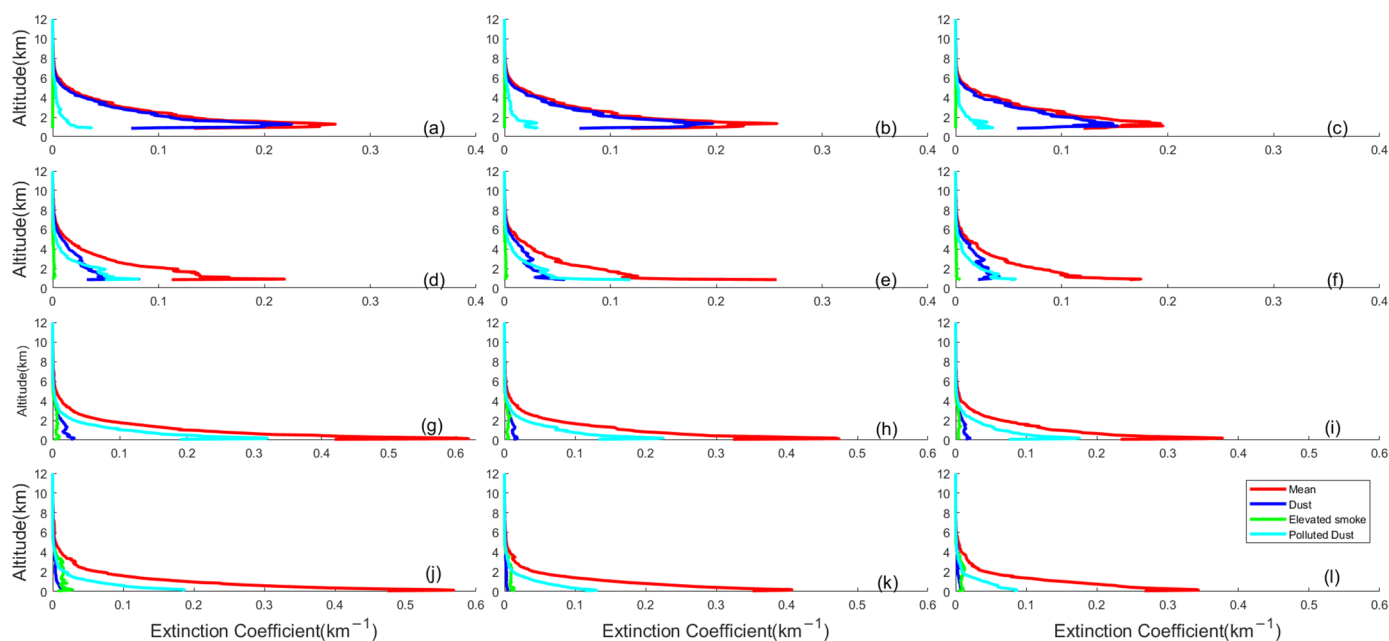


Figure 9. Seasonal vertical distribution of average extinction coefficient (red solid line), dust extinction coefficient (blue solid line), Elevated smoke extinction coefficient (green solid line), and Polluted dust extinction coefficient (cyan solid line) for Taklimakan Desert (TD) (a–c), North central region of China (NCR) (d–f), North China Plain (NCP) (g–i), and Yangtze River Delta (YRD) (j–l) for 2007–2013, 2014–2018, and 2019–2020.

We found that the annual-average variation of OF of different types of aerosols in different regions since the implementation of the pollution control policy is not obvious (Figure 10). However, what can be clearly seen is that the OF of polluted dust and dust aerosols are higher in different regions, and the regions with the smallest variation in the OF of different types of aerosols from 2007 to 2020 are TD and NCR, whose OF of perennial dust aerosols is higher than 0.7 and 0.55, respectively. Besides dust and polluted dust aerosol, polluted continent/smoke and elevated smoke aerosol mainly occur in TD and NCR. The aerosol types observed for NCP and YRD are more complex, and the annual-average variation of OF of different types of aerosols in NCP is more stable, while the decreasing trend of OF of clean marine and dusty marine in YRD is more obvious. In summary, it can be seen that the polluted dust AOD and different altitude extinction coefficient of NCP and YRD decreased significantly, but the reason their OF did not decrease significantly may be mainly due to the more rapid decrease of other types of extinction coefficient values. It also indicates that pollution control policies may not have led to a reduction in anthropogenic aerosols (e.g., raw coal use) in some regions. This is consistent with the findings of Jin et al. [74].

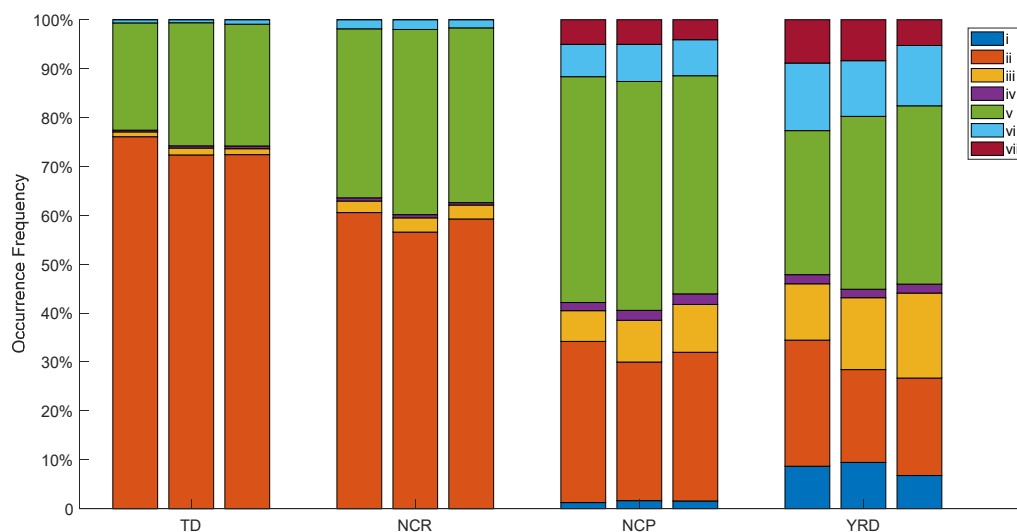


Figure 10. Average occurrence frequency (OF) for seven aerosol types in China for 2007–2013, 2014–2018, and 2019–2020. three columns for each region indicate 2007–2013, 2014–2018, and 2019–2020, respectively. Letters i–vii represent clean marine, dust, polluted continental/smoke, clean continental, polluted dust, elevated smoke, and dusty marine.

4.2. Analysis of the Variation of Aerosol Properties in the Study Area by Longitude

The variation of AOD and vertical distribution and vertical transport of extinction coefficient for the dominant aerosols in the selected study areas were determined, as well as the distribution of all, dust, elevated smoke, polluted dust AOD and extinction coefficient with longitude for TP, NCR, NCP, and YRD (Figures 11 and 12). Furthermore, different types of aerosol OF variations with longitude for TP, NCR, NCP, and YRD were plotted (Figure 13). There are obvious AOD variations between regions, and there are some variations in the dominant aerosol types in different areas, while the aerosol type changes with longitude. The maximum value of all extinction coefficient appears at the ground level, and gradually decreases with increasing altitude, and there is no obvious value of extinction coefficient above 8 km for any extinction coefficient in the any of the regions.

In the TD, the all AOD and dust AOD vary in tandem, both increasing and then decreasing, while in the middle of the TD the dust AOD is larger than that of the either the east or west of the TD, but the polluted dust AOD is slightly lower than in the east and west of TD, as evidenced by the longitudinal variation of aerosol type OF. In the middle of TD the dust aerosol OF is the largest, and the polluted dust aerosol OF is lower than in the east and west of TD which is consistent with the extinction coefficient distribution. The TD dust extinction coefficient is consistent with the all-extinction coefficient variation, while it is also affected by polluted dust, which is mainly below 3 km in central TD. In the western part of the NCR, the dust aerosol decreases significantly and the all-extinction coefficient appears briefly low at 2–3 km and then high again near 4 km, which can be found in combination with the vertical distribution of TD dust extinction coefficient, which is related to TD dust transport. It is shown that the dust transport of TD is more related to high altitude (above 4 km) than below 4 km [33,34]. In the eastern part of the NCR, dust aerosol changes gradually decrease, elevated smoke aerosol starts to appear, polluted continental/smoke OF gradually increases, and polluted dust AOD appears high, which may be related to the economic development and topography in the eastern part of NCR, and the near-surface westerly winds in the western area of the eastern part of the NCR will transport pollutants to the east. The topography of Guanzhong Plain, which is wide in the east and narrow in the west and surrounded by mountains on three sides, is not conducive to the diffusion of pollutants, resulting in the accumulation of pollutants in the eastern part [75,76]. Simultaneously, the pollution problems caused by industrial

pollution and traffic emissions in the eastern part of the NCR, mainly in Xi'an, also play a role [77]. This is also indicated by the higher OF of high smoke aerosol and polluted dust in the eastern NCR. The main aerosol type in the NCP is polluted dust aerosol, the polluted dust AOD and all AOD in this area are more consistent, and the high value of polluted dust extinction coefficient mainly occurring below 4 km. With the change of longitude NCP dust AOD value gradually decreases, elevated smoke AOD starts to increase, and the OF of dust aerosol and elevated smoke aerosol also gradually increases. And elevated smoke extinction coefficient is higher near 2 km in the eastern region of NCP, and the OF of elevated smoke aerosol is also larger, which may be related to the more frequent human activities in the Beijing-Tianjin-Hebei region. In contrast, YRD differs from the other three study regions in that elevated smoke aerosols also contribute more to air pollution in this region in addition to polluted dust aerosols, and the extinction coefficient of elevated smoke aerosols have a stronger vertical distribution range. The YRD dust AOD gradually decreased near the ocean, and elevated smoke and polluted dust AOD appeared to rise briefly with increasing longitude and then start to decline. The main aerosol types of polluted continental/smoke, clean continental, and polluted dust OF gradually decrease with longitude change, and then the main aerosol types of OF gradually increase are clean marine and dusty marine. The polluted dust extinction coefficients of YRD change in steps of 0–2 km, 2–4 km, and 4–6 km, while the elevated smoke extinction coefficient values in this region are higher below 4 km, and then increase slightly above 6 km after the decrease of elevated smoke extinction coefficient coefficients from 5–6 km.

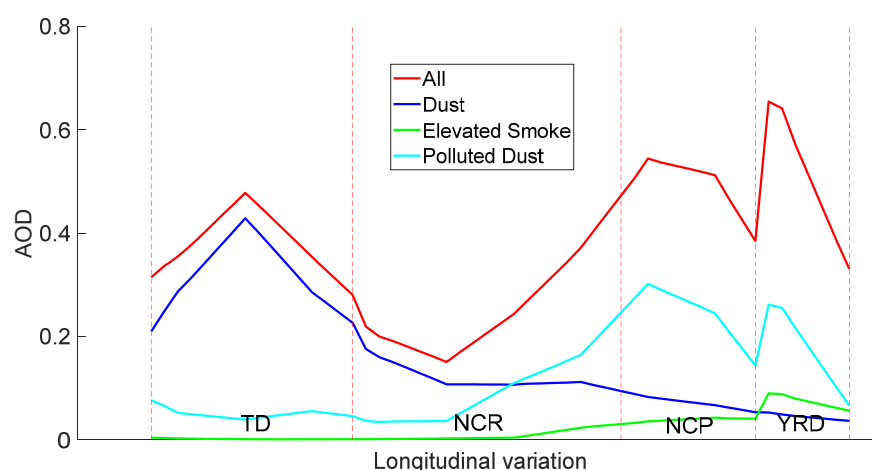
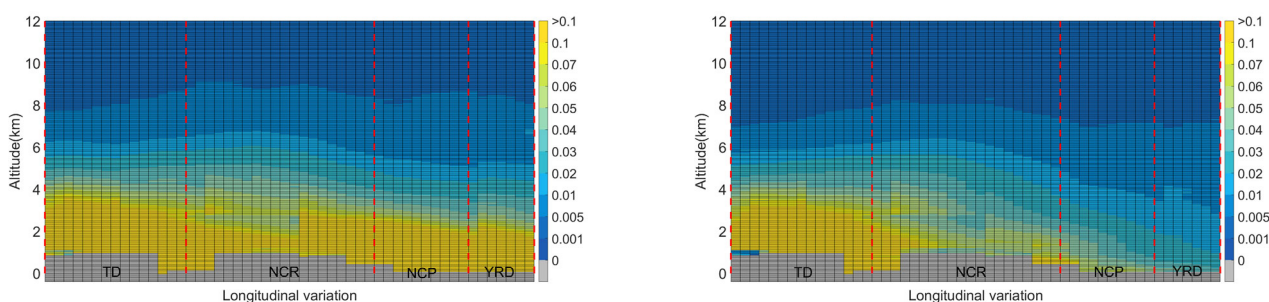


Figure 11. Taklimakan Desert (TD, 75.5–90.5° E), North central region of China (NCR, 90.5–110.5° E), North China Plain (NCP, 110.5–120.5° E), and Yangtze River Delta (YRD, 116.5–122.5° E) with longitude all, dust, elevated smoke, polluted dust aerosol optical depth (AOD).



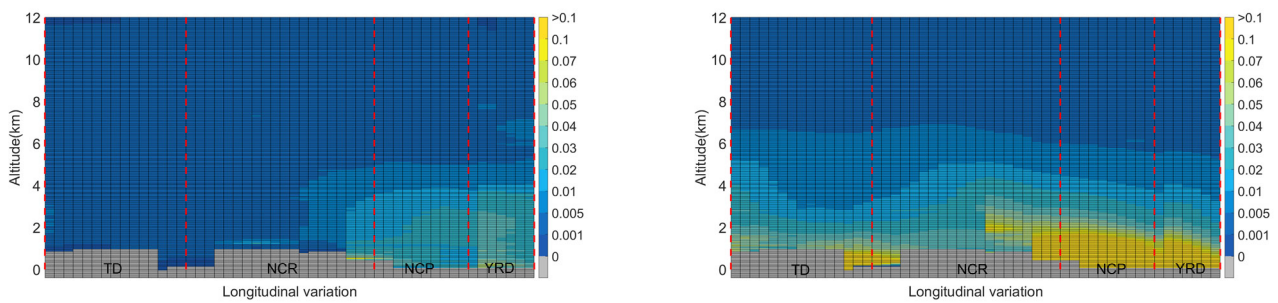


Figure 12. Longitudinal variation of the decadal mean extinction coefficient for All-aerosol, dust, elevated smoke, polluted dust over Taklimakan Desert (TD, 75.5–90.5° E), North central region of China (NCR, 90.5–110.5° E), North China Plain (NCP, 110.5–120.5° E), and Yangtze River Delta (YRD, 116.5–122.5° E).

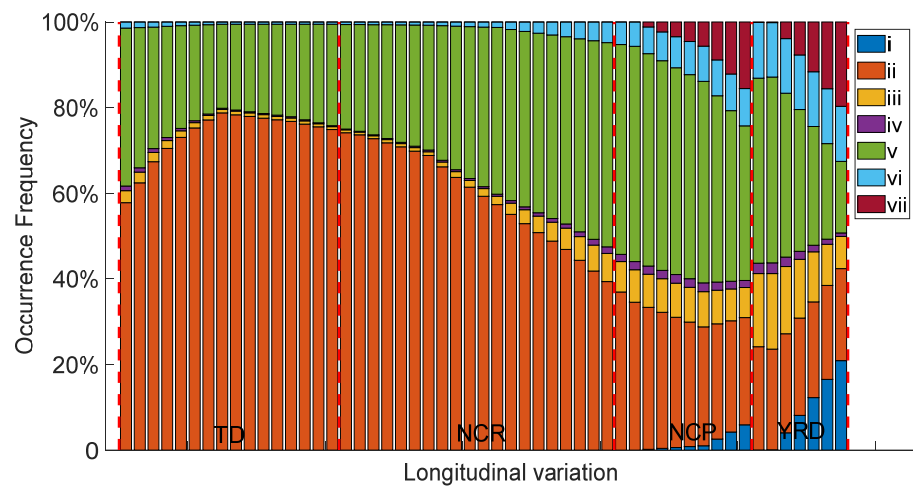


Figure 13. 2007–2020 Occurrence Frequency (OF) changes of seven aerosol types of Taklimakan Desert (TD, 75.5–90.5° E), North central region of China (NCR, 90.5–110.5° E), North China Plain (NCP, 110.5–120.5° E), and Yangtze River Delta (YRD, 116.5–122.5° E). Letters i–vii represent clean marine, dust, polluted continental/smoke, clean continental, polluted dust, elevated smoke, and dusty marine.

5. Conclusions

The horizontal and vertical distributions of TD, NCR, NCP, and YRD aerosol properties were studied using CALIPSO L3 aerosol data from 2007 to 2020, and the effects of China's pollution control policies on AOD, aerosol types and extinction coefficients in the study area were analyzed. The main findings of this paper are as follows.

The distribution of AOD in TD, NCR, NCP, and YRD has obvious spatial and seasonal differences. In general, high values of all AOD are in TD, NCP and YRD. There is an obvious diffusion of dust aerosol in northern China during MAM, and the spatial distribution of polluted dust AOD values are centered on the NCP. Furthermore, the concentration of polluted dust aerosol decreases irregularly as the distance from the NCP increases. China's pollution prevention and control policies have a strong influence on regional all AOD values, and NCP is more responsive to pollution prevention and control policies. TD, NCR, NCP, and YRD have 5%, 13.8%, 15.5%, and 23.7% decline rates in all AOD in 2014–2018 compared to 2007–2013, and decline rates of 7.8%, 11.5%, 16%, and 10.4% in 2019–2020 compared to 2014–2018.

The extinction coefficient distributions showed significant spatial and temporal differences in TD, NCR, NCP, YRD regions and different altitude extinction coefficient distributions. At 0–12 km, NCP and YRD total extinction coefficient had a wider vertical

distribution than TD and NCR, and the seasonal variation of all extinction coefficient was also weaker than TD and NCR. The only exception was TD, where the dominant aerosol type was dust throughout the year, the dominant aerosol types in the other three regions vary somewhat in different seasons. Influenced by the pollution prevention policy, the extinction coefficient shows a significant trend of decrease in the interval from 2014–2018 and 2019–2020 compared to the pre-2014 period.

The multi-year average distribution of seven aerosol type OF from 2007–2020 was also calculated, and we found that there were significant spatial differences in different aerosol type OF. However, the inter-annual variation of different types of aerosol OF in each region was not significantly affected by pollution prevention and control policies. The largest OF of dust aerosol was in the TD and western NCR. The TD has the highest OF of polluted dust in DJF, reaching 39.4%. Polluted dust aerosols are evident throughout the year in NCP, while elevated smoke aerosols are second only to polluted dust aerosols in JJA, and dust aerosols are second only to polluted dust aerosols in SON and DJF. The seasonal OF trends of NCP polluted continental/smoke, clean continental, and elevated smoke aerosol types are consistent, all decreasing after the highest value during JJA. The dominant aerosol types in YRD MAM are dust and polluted dust aerosols, while JJA present polluted continental/smoke and elevated smoke aerosols with higher OF, and the most obvious aerosol type during SON and DJF is polluted dust. When comparing UVAI and SSA distributions with the aerosol types obtained from CALIPSO, it was found that the aerosol property profiles expressed by UVAI and SSA strongly corroborated the aerosol types obtained from CALIPSO. The inter-annual variation of different types of aerosol OF in each region was not significantly influenced by pollution control policies.

Finally, we analyzed the relationship between aerosol optical properties and longitude in the study area, and found that TD, NCR, NCP, and YRD showed a significant decrease of dust aerosol and an increase of polluted dust aerosol with the change of longitude. And starting from NCR, polluted continental/smoke and elevated smoke aerosol OF also started to increase. The magnitude of extinction coefficients at different altitudes also showed that the long-range transport of TD and NCR dust aerosols at high altitudes had a substantial impact on NCP and YRD. Furthermore, OF gradually decreases with longitude change, and the aerosol types with gradually increasing OF are mainly clean marine and dusty marine, which proves the similarities of aerosol type and longitude change in the study area.

Author Contributions: Conceptualization, K.L.; Data curation, Z.C.; Formal analysis, Z.C.; Investigation, K.L.; Methodology, K.L.; Resources, Z.C., S.H., Z.Q. and Z.W.; Software, K.L.; Supervision, S.H., Z.Q. and Z.W.; Validation, W.S. and Z.H.; Visualization, W.S. and Z.H.; Writing—original draft, Z.C.; Writing—review & editing, K.L. All authors have read and agreed to the published version of the manuscript.

Funding: This research was funded by Shanghai Ocean Bureau Research Project (Shanghai 2019-05).

Data Availability Statement: CALIPSO datasets are available online at the NASA Giovanni site (<https://www-calipso.larc.nasa.gov>, accessed on 1 January 2022). MODIS AOD datasets are available online at the NASA Giovanni site (<https://giovanni.gsfc.nasa.gov/giovanni>, accessed on 10 August 2021). OMI AOD datasets are available online at the NASA Giovanni site (<https://www.earthdata.nasa.gov/>, accessed on 10 October 2021).

Acknowledgments: The authors are sincerely grateful for the data support from NASA.

Conflicts of Interest: The authors declare no conflict of interest.

References

1. Jinxi, C.; Rong, L.; Minghui, T.; Lili, W.; Changqing, L.; Jun, W.; Lunche, W.; Yi, W.; Liangfu, C. Overview of the performance of satellite fire products in china: Uncertainties and challenges. *Atmos. Environ.* **2022**, *268*, 118838.
2. Zhou, B.; Chao, Q.; Huang, L. The Core Conclusions and Interpretation of Working Group I Contribution to the Fifth Assessment Report of the Intergovernmental Panel on Climate Change. *Chin. J. Urban Environ. Stud.* **2015**, *3*, 1550003. <https://doi.org/10.1142/s2345748115500037>.

3. Ahn, S.H.; Yoon, Y.; Choi, T.; Lee, J.; Kim, Y.; Lee, B.; Ritter, C.; Aas, W.; Krejci, R.; Ström, J.; et al. Relationship between cloud condensation nuclei (CCN) concentration and aerosol optical depth in the Arctic region. *Atmospheric Environ.* **2021**, *267*, 118748. <https://doi.org/10.1016/j.atmosenv.2021.118748>.
4. Charlson, R.J.; Schwartz, S.E.; Hales, J.M.; Cess, R.D.; Coakley Jr, J.A.; Hansen, J.E.; Hofmann, D.J. Climate forcing by anthropogenic aerosols. *Science* **1992**, *255*, 423–430.
5. Wei, X.; Chang, N.-B.; Bai, K.; Gao, W. Satellite remote sensing of aerosol optical depth: Advances, challenges, and perspectives. *Crit. Rev. Environ. Sci. Technol.* **2020**, *50*, 1640–1725. <https://doi.org/10.1080/10643389.2019.1665944>.
6. Torres, O.; Tanskanen, A.; Veihelmann, B.; Ahn, C.; Braak, R.; Bhartia, P.; Veeffkind, P.; Levelt, P.P. Aerosols and surface UV products from Ozone Monitoring Instrument observations: An overview. *J. Geophys. Res. Atmos.* **2007**, *112*, D24S47. <https://doi.org/10.1029/2007jd008809>.
7. Jung, C.H.; Lee, J.Y.; Um, J.; Lee, S.S.; Yoon, Y.J.; Kim, Y.P. Estimation of Source-Based Aerosol Optical Properties for Polydisperse Aerosols from Receptor Models. *Appl. Sci.* **2019**, *9*, 1443. <https://doi.org/10.3390/app9071443>.
8. Si, Y.; Chen, L.; Xiong, X.; Shi, S.; Husi, L.; Cai, K. Evaluation of the MISR fine resolution aerosol product using MODIS, MISR, and ground observations over China. *Atmospheric Environ.* **2019**, *223*, 117229. <https://doi.org/10.1016/j.atmosenv.2019.117229>.
9. Wei, J.; Li, Z.; Sun, L.; Peng, Y.; Liu, L.; He, L.; Qin, W.; Cribb, M. MODIS Collection 6.1 3 km resolution aerosol optical depth product: Global evaluation and uncertainty analysis. *Atmospheric Environ.* **2020**, *240*, 117768. <https://doi.org/10.1016/j.atmosenv.2020.117768>.
10. Huneus, N.; Schulz, M.; Balkanski, Y.; Griesfeller, J.; Prospero, J.; Kinne, S.; Bauer, S.; Boucher, O.; Chin, M.; Dentener, F.; et al. Global dust model intercomparison in AeroCom phase I. *Atmospheric Meas. Technol.* **2011**, *11*, 7781–7816. <https://doi.org/10.5194/acp-11-7781-2011>.
11. Winker, D.M.; Hunt, W.H.; McGill, M.J. Initial performance assessment of CALIOP. *Geophys. Res. Lett.* **2007**, *34*, L19803. <https://doi.org/10.1029/2007gl030135>.
12. IPCC; Stocker, T.F.; Qin, D.; Plattner, G.K.; Midgley, P.M. The physical science basis. In *Contribution of Working Group I to the Fifth Assessment Report of the Intergovernmental Panel on Climate Change*; Cambridge University Press: Cambridge, UK, 2013; p. 2013.
13. Tomasi, C.; Kokhanovsky, A.A.; Lupi, A.; Ritter, C.; Smirnov, A.; O'Neill, N.T.; Stone, R.S.; Holben, B.N.; Nyeki, S.; Wehrli, C.; et al. Aerosol remote sensing in polar regions. *Earth-Science Rev.* **2015**, *140*, 108–157. <https://doi.org/10.1016/j.earsci-rev.2014.11.001>.
14. Xie, Y.; Li, Z.; Li, L.; Wagener, R.; Abboud, I.; Li, K.; Li, D.; Zhang, Y.; Chen, X.; Xu, H. Aerosol optical, microphysical, chemical and radiative properties of high aerosol load cases over the Arctic based on AERONET measurements. *Sci. Rep.* **2018**, *8*, 9376. <https://doi.org/10.1038/s41598-018-27744-z>.
15. Prasad, A.K.; Singh, S.; Chauhan, S.; Srivastava, M.K.; Singh, R. Aerosol radiative forcing over the Indo-Gangetic plains during major dust storms. *Atmospheric Environ.* **2007**, *41*, 6289–6301. <https://doi.org/10.1016/j.atmosenv.2007.03.060>.
16. Soni, M.; Verma, S.; Jethava, H.; Payra, S.; Lamsal, L.; Gupta, P.; Singh, J. Impact of COVID-19 on the Air Quality over China and India Using Long-term (2009–2020) Multi-satellite Data. *Aerosol Air Qual. Res.* **2021**, *21*, 200295. <https://doi.org/10.4209/aaqr.2020.06.0295>.
17. Bibi, H.; Alam, K.; Chishtie, F.; Bibi, S.; Shahid, I.; Blaschke, T. Intercomparison of MODIS, MISR, OMI, and CALIPSO aerosol optical depth retrievals for four locations on the Indo-Gangetic plains and validation against AERONET data. *Atmospheric Environ.* **2015**, *111*, 113–126. <https://doi.org/10.1016/j.atmosenv.2015.04.013>.
18. Ali, A.; Amin, S.E.; Ramadan, H.H.; Tolba, M.F. Enhancement of OMI aerosol optical depth data assimilation using artificial neural network. *Neural Comput. Appl.* **2012**, *23*, 2267–2279. <https://doi.org/10.1007/s00521-012-1178-9>.
19. Hsu, N.C.; Lee, J.; Sayer, A.M.; Carletta, N.; Chen, S.; Tucker, C.J.; Holben, B.N.; Tsay, S. Retrieving near-global aerosol loading over land and ocean from AVHRR. *J. Geophys. Res. Atmos.* **2017**, *122*, 9968–9989. <https://doi.org/10.1002/2017jd026932>.
20. Li, Y.; Shi, G.; Sun, Z. Evaluation and improvement of MODIS aerosol optical depth products over China. *Atmospheric Environ.* **2019**, *223*, 117251. <https://doi.org/10.1016/j.atmosenv.2019.117251>.
21. Jääskeläinen, E.; Manninen, T.; Tamminen, J.; Laine, M. The Aerosol Index and Land Cover Class Based Atmospheric Correction Aerosol Optical Depth Time Series 1982–2014 for the SMAC Algorithm. *Remote Sens.* **2017**, *9*, 1095. <https://doi.org/10.3390/rs9111095>.
22. Zhu, J.; Xia, X.; Wang, J.; Che, H.; Chen, H.; Zhang, J.; Xu, X.; Levy, R.C.; Oo, M.; Holz, R.; et al. Evaluation of Aerosol Optical Depth and Aerosol Models from VIIRS Retrieval Algorithms over North China Plain. *Remote Sens.* **2017**, *9*, 432. <https://doi.org/10.3390/rs9050432>.
23. Bibi, S.; Alam, K.; Chishtie, F.; Bibi, H. Characterization of absorbing aerosol types using ground and satellites based observations over an urban environment. *Atmospheric Environ.* **2017**, *150*, 126–135. <https://doi.org/10.1016/j.atmosenv.2016.11.052>.
24. Sabetghadam, S.; Alizadeh, O.; Khoshsima, M.; Pierleoni, A. Aerosol properties, trends and classification of key types over the Middle East from satellite-derived atmospheric optical data. *Atmospheric Environ.* **2020**, *246*, 118100. <https://doi.org/10.1016/j.atmosenv.2020.118100>.
25. Kumar, K.R.; Kang, N.; Yin, Y. Classification of key aerosol types and their frequency distributions based on satellite remote sensing data at an industrially polluted city in the Yangtze River Delta, China. *Int. J. Clim.* **2017**, *38*, 320–336. <https://doi.org/10.1002/joc.5178>.

26. Bilal, M.; Ali, A.; Nichol, J.E.; Bleiweiss, M.P.; de Leeuw, G.; Mhawish, A.; Shi, Y.; Mazhar, U.; Mehmood, T.; Kim, J.; et al. AEROSol generic classification using a novel Satellite remote sensing Approach (AEROSA). *Front. Environ. Sci.* **2022**, *10*, 981522. <https://doi.org/10.3389/fenvs.2022.981522>.
27. Winker, D.M.; Vaughan, M.A.; Omar, A.; Hu, Y.; Powell, K.A.; Liu, Z.; Hunt, W.H.; Young, S.A. Overview of the CALIPSO Mission and CALIOP Data Processing Algorithms. *J. Atmospheric Ocean. Technol.* **2009**, *26*, 2310–2323. <https://doi.org/10.1175/2009jtecha1281.1>.
28. Tackett, J.L.; Winker, D.M.; Getzewich, B.J.; Vaughan, M.A.; Young, S.A.; Kar, J. CALIPSO lidar level 3 aerosol profile product: Version 3 algorithm design. *Atmos. Meas. Technol.* **2018**, *11*, 4129–4152. <https://doi.org/10.5194/amt-11-4129-2018>.
29. Pan, H.; Huang, J.; Kumar, K.R.; An, L.; Zhang, J. The CALIPSO retrieved spatiotemporal and vertical distributions of AOD and extinction coefficient for different aerosol types during 2007–2019: A recent perspective over global and regional scales. *Atmos. Environ.* **2022**, *274*, 118986. <https://doi.org/10.1016/j.atmosenv.2022.118986>.
30. Mehta, M.; Singh, N.; Anshumali Global trends of columnar and vertically distributed properties of aerosols with emphasis on dust, polluted dust and smoke—Inferences from 10-year long CALIOP observations. *Remote Sens. Environ.* **2018**, *208*, 120–132. <https://doi.org/10.1016/j.rse.2018.02.017>.
31. Yang, Y.; Zhao, C.; Wang, Q.; Cong, Z.; Yang, X.; Fan, H. Aerosol characteristics at the three poles of the Earth as characterized by Cloud–Aerosol Lidar and Infrared Pathfinder Satellite Observations. *Atmos. Meas. Technol.* **2021**, *21*, 4849–4868. <https://doi.org/10.5194/acp-21-4849-2021>.
32. Gui, L.; Tao, M.; Wang, Y.; Wang, L.; Chen, L.; Lin, C.; Tao, J.; Wang, J.; Yu, C. Climatology of aerosol types and their vertical distribution over East Asia based on CALIPSO lidar measurements. *Int. J. Clim.* **2022**, *42*, 6042–6054. <https://doi.org/10.1002/joc.7599>.
33. Chen, S.; Huang, J.; Li, J.; Jia, R.; Jiang, N.; Kang, L.; Ma, X.; Xie, T. Comparison of dust emissions, transport, and deposition between the Taklimakan Desert and Gobi Desert from 2007 to 2011. *Sci. China Earth Sci.* **2017**, *60*, 1338–1355. <https://doi.org/10.1007/s11430-016-9051-0>.
34. Nan, Y.; Wang, Y. De-coupling interannual variations of vertical dust extinction over the Taklimakan Desert during 2007–2016 using CALIOP. *Sci. Total. Environ.* **2018**, *633*, 608–617. <https://doi.org/10.1016/j.scitotenv.2018.03.125>.
35. Liu, G.; Li, J.; Jiang, Z.; Li, X. Impact of sea surface temperature variability at different ocean basins on dust activities in the Gobi Desert and North China. *Geophys. Res. Lett.* **2022**, *49*, e2022GL099821. <https://doi.org/10.1029/2022gl099821>.
36. de Leeuw, G.; Sogacheva, L.; Rodriguez, E.; Kourtidis, K.; Georgoulas, A.K.; Alexandri, G.; Amiridis, V.; Proestakis, E.; Marinou, E.; Xue, Y.; et al. Two decades of satellite observations of AOD over mainland China using ATSR-2, AATSR and MODIS/Terra: Data set evaluation and large-scale patterns. *Atmos. Meas. Technol.* **2018**, *18*, 1573–1592. <https://doi.org/10.5194/acp-18-1573-2018>.
37. Kang, N.; Kumar, K.R.; Hu, K.; Yu, X.; Yin, Y. Long-term (2002–2014) evolution and trend in Collection 5.1 Level-2 aerosol products derived from the MODIS and MISR sensors over the Chinese Yangtze River Delta. *Atmos. Res.* **2016**, *181*, 29–43. <https://doi.org/10.1016/j.atmosres.2016.06.008>.
38. Kang, H.; Zhu, B.; Liu, X.; Shi, S.; Hou, X.; Lu, W.; Yan, S.; Pan, C.; Chen, Y. Three-Dimensional Distribution of PM_{2.5} over the Yangtze River Delta as Cold Fronts Moving Through. *J. Geophys. Res. Atmos.* **2021**, *126*, e2020JD034035. <https://doi.org/10.1029/2020jd034035>.
39. Liu, C.; Shen, X.; Gao, W. Intercomparison of CALIOP, MODIS, and AERONET aerosol optical depth over China during the past decade. *Int. J. Remote Sens.* **2018**, *39*, 7251–7275. <https://doi.org/10.1080/01431161.2018.1466070>.
40. Wang, P.; Ning, S.; Dai, J.; Sun, J.; Lv, M.; Song, Q.; Dai, X.; Zhao, J.; Yu, D. Trends and Variability in Aerosol Optical Depth over North China from MODIS C6 Aerosol Products during 2001–2016. *Atmosphere* **2017**, *8*, 223. <https://doi.org/10.3390/atmos8110223>.
41. Quan, J.; Zhang, Q.; He, H.; Liu, J.; Huang, M.; Jin, H. Analysis of the formation of fog and haze in North China Plain (NCP). *Atmospheric Meas. Technol.* **2011**, *11*, 8205–8214. <https://doi.org/10.5194/acp-11-8205-2011>.
42. Liu, B.; Ma, Y.; Gong, W.; Zhang, M.; Wang, W.; Shi, Y. Comparison of AOD from CALIPSO, MODIS, and Sun Photometer under Different Conditions over Central China. *Sci. Rep.* **2018**, *8*, 10066. <https://doi.org/10.1038/s41598-018-28417-7>.
43. Liu, C.; Yin, Z.; He, Y.; Wang, L. Climatology of Dust Aerosols over the Jiangnan Plain Revealed with Space-Borne Instruments and MERRA-2 Reanalysis Data during 2006–2021. *Remote Sens.* **2022**, *14*, 4414. <https://doi.org/10.3390/rs14174414>.
44. Mao, Q.; Huang, C.; Zhang, H.; Chen, Q.; Yuan, Y. Performance of MODIS aerosol products at various timescales and in different pollution conditions over eastern Asia. *Sci. China Technol. Sci.* **2020**, *64*, 774–784. <https://doi.org/10.1007/s11431-018-9462-5>.
45. Yang, L.; Tian, X.; Liu, C.; Ji, W.; Zheng, Y.; Liu, H.; Lu, X.; Che, H. Evaluation and Comparison of MODIS C6 and C6.1 Deep Blue Aerosol Products in Arid and Semi-Arid Areas of Northwestern China. *Remote Sens.* **2022**, *14*, 1935. <https://doi.org/10.3390/rs14081935>.
46. Wang, Y.; Yuan, Q.; Shen, H.; Zheng, L.; Zhang, L. Investigating multiple aerosol optical depth products from MODIS and VIIRS over Asia: Evaluation, comparison, and merging. *Atmospheric Environ.* **2020**, *230*, 117548. <https://doi.org/10.1016/j.atmosenv.2020.117548>.
47. Levelt, P.F.; Hilsenrath, E.; Leppelmeier, G.W.; van den Oord, G.H.J.; Bhartia, P.K.; Tamminen, J.; De Haan, J.F.; Veefkind, J.P. Science objectives of the ozone monitoring instrument. *IEEE Trans. Geosci. Remote Sens.* **2006**, *44*, 1199–1208. <https://doi.org/10.1109/tgrs.2006.872336>.
48. Zhang, W.; Gu, X.; Xu, H.; Yu, T.; Zheng, F. Assessment of OMI near-UV aerosol optical depth over Central and East Asia. *J. Geophys. Res. Atmos.* **2016**, *121*, 382–398. <https://doi.org/10.1002/2015jd024103>.

49. Ahn, C.; Torres, O.; Bhartia, P. Comparison of Ozone Monitoring Instrument UV Aerosol Products with Aqua/Moderate Resolution Imaging Spectroradiometer and Multiangle Imaging Spectroradiometer observations in 2006. *J. Geophys. Res. Atmos.* **2008**, *113*, D16S27. <https://doi.org/10.1029/2007jd008832>.
50. De Meij, A.; Pozzer, A.; Lelieveld, J. Global and regional trends in aerosol optical depth based on remote sensing products and pollutant emission estimates between 2000 and 2009. *Atmos. Chem. Phys.* **2010**, *10*, 30731–30776.
51. Ali, A.; Amin, S.E.; Ramadan, H.H.; Tolba, M.F. Ozone Monitoring Instrument aerosol products: A comparison study with ground-based airborne sun photometer measurements over Europe. *Int. J. Remote Sens.* **2012**, *33*, 6321–6341. <https://doi.org/10.1080/01431161.2012.685526>.
52. Zheng, J.; Zhang, Z.; Garnier, A.; Yu, H.; Song, Q.; Wang, C.; Dubuisson, P.; Di Biagio, C. The thermal infrared optical depth of mineral dust retrieved from integrated CALIOP and IIR observations. *Remote Sens. Environ.* **2021**, *270*, 112841. <https://doi.org/10.1016/j.rse.2021.112841>.
53. Jzad, E.; Xxa, B.; Hc, C.; Jw, D.; Jza, B.; Yd, F. Study of aerosol optical properties at kunming in southwest china and long-range transport of biomass burning aerosols from north burma. *Atmos. Res.* **2016**, *169*, 237–247.
54. Ramanathan, V.; Ramana, M.V.; Roberts, G.; Kim, D.; Corrigan, C.; Chung, C.; Winker, D.M. Warming trends in Asia amplified by brown cloud solar absorption. *Nature* **2007**, *448*, 575–578. <https://doi.org/10.1038/nature06019>.
55. Liu, P.F.; Zhao, C.S.; Göbel, T.; Hallbauer, E.; Nowak, A.; Ran, L.; Xu, W.Y.; Deng, Z.Z.; Ma, N.; Mildenerberger, K.; et al. Hygroscopic properties of aerosol particles at high relative humidity and their diurnal variations in the North China Plain. *Atmospheric Meas. Technol.* **2011**, *11*, 3479–3494. <https://doi.org/10.5194/acp-11-3479-2011>.
56. Sun, Y.; Jiang, Q.; Xu, Y.; Ma, Y.; Zhang, Y.; Liu, X.; Li, W.; Wang, F.; Li, J.; Wang, P.; et al. Aerosol characterization over the North China Plain: Haze life cycle and biomass burning impacts in summer. *J. Geophys. Res. Atmos.* **2016**, *121*, 2508–2521. <https://doi.org/10.1002/2015jd024261>.
57. Zhao, X.J.; Zhao, P.S.; Xu, J.; Meng, W.; Pu, W.W.; Dong, F.; He, D.; Shi, Q.F. Analysis of a winter regional haze event and its formation mechanism in the North China Plain. *Atmospheric Meas. Technol.* **2013**, *13*, 5685–5696. <https://doi.org/10.5194/acp-13-5685-2013>.
58. Yang, Y.R.; Liu, X.G.; Qu, Y.; An, J.L.; Jiang, R.; Zhang, Y.H.; Sun, Y.L.; Wu, Z.J.; Zhang, F.; Xu, W.Q.; et al. Characteristics and formation mechanism of continuous hazes in China: A case study during the autumn of 2014 in the North China Plain. *Atmospheric Meas. Technol.* **2015**, *15*, 8165–8178. <https://doi.org/10.5194/acp-15-8165-2015>.
59. Li, J.; Hao, X.; Liao, H.; Wang, Y.; Cai, W.; Li, K.; Yue, X.; Yang, Y.; Chen, H.; Mao, Y.; et al. Winter particulate pollution severity in North China driven by atmospheric teleconnections. *Nat. Geosci.* **2022**, *15*, 349–355. <https://doi.org/10.1038/s41561-022-00933-2>.
60. Omar, A.H.; Winker, D.M.; Vaughan, M.A.; Hu, Y.; Trepte, C.R.; Ferrare, R.A.; Lee, K.-P.; Hostetler, C.A.; Kittaka, C.; Rogers, R.R.; et al. The CALIPSO Automated Aerosol Classification and Lidar Ratio Selection Algorithm. *J. Atmospheric Ocean. Technol.* **2009**, *26*, 1994–2014. <https://doi.org/10.1175/2009jtecha1231.1>.
61. Ding, A.J.; Fu, C.B.; Yang, X.Q.; Sun, J.N.; Zheng, L.F.; Xie, Y.N.; Herrmann, E.; Nie, W.; Petäjä, T.; Kerminen, V.-M.; et al. Ozone and fine particle in the western Yangtze River Delta: An overview of 1 yr data at the SORPES station. *Atmospheric Meas. Technol.* **2013**, *13*, 5813–5830. <https://doi.org/10.5194/acp-13-5813-2013>.
62. Fu, Q.; Zhuang, G.; Li, J.; Huang, K.; Wang, Q.; Zhang, R.; Fu, J.; Lu, T.; Chen, M.; Wang, Q.; et al. Source, long-range transport, and characteristics of a heavy dust pollution event in Shanghai. *J. Geophys. Res. Atmos.* **2010**, *115*, D00K29. <https://doi.org/10.1029/2009jd013208>.
63. Tian, X.; Xie, P.; Xu, J.; Li, A.; Wang, Y.; Qin, M.; Hu, Z. Long-term observations of tropospheric NO₂, SO₂ and HCHO by MAX-DOAS in Yangtze River Delta area, China. *J. Environ. Sci.* **2018**, *71*, 207–221. <https://doi.org/10.1016/j.jes.2018.03.006>.
64. Hammer, M.S.; Martin, R.V.; Li, C.; Torres, O.; Manning, M.; Boys, B.L. Insight into global trends in aerosol composition from 2005 to 2015 inferred from the OMI Ultraviolet Aerosol Index. *Atmospheric Meas. Technol.* **2018**, *18*, 8097–8112. <https://doi.org/10.5194/acp-18-8097-2018>.
65. Hammer, M.S.; Martin, R.V.; van Donkelaar, A.; Buchard, V.; Torres, O.; Ridley, D.A.; Spurr, R.J.D. Interpreting the ultraviolet aerosol index observed with the OMI satellite instrument to understand absorption by organic aerosols: Implications for atmospheric oxidation and direct radiative effects. *Atmospheric Meas. Technol.* **2016**, *16*, 2507–2523. <https://doi.org/10.5194/acp-16-2507-2016>.
66. Kang, Y.; Wang, L.L.; Xin, J.Y. Analysis of the Change Trend of Aerosol Single-Scattering Albedo in the Areas of Northern China Based on AERONET and OMI Data. *Clim. Environ. Res.* **2019**, *24*, 537–551. <https://doi.org/10.3878/j.issn.1006-9585.2018.18006>.
67. Jin, Q.; Fang, X.; Wen, B.; Shan, A. Spatio-temporal variations of pm_{2.5} emission in china from 2005 to 2014. *Chemosphere: Environ. Toxicol. Risk Assess.* **2017**, *183*, 429–436.
68. Xs, A.; Yz, A.; Yu, L.; Wxa, B.; Gang, Y.; Xin, L.; Bc, C.; Dan, T.; Jwa, B. Air quality benefits of achieving carbon neutrality in china. *Sci. Total Environ.* **2021**, *795*, 148784.
69. Chen, Y.; Schleicher, N.; Chen, Y.; Chai, F.; Norra, S. The influence of governmental mitigation measures on contamination characteristics of PM_{2.5} in Beijing. *Sci. Total Environ.* **2014**, *490*, 647–658. <https://doi.org/10.1016/j.scitotenv.2014.05.049>.
70. Yuan, X.; Zhang, M.; Wang, Q.; Wang, Y.; Zuo, J. Evolution analysis of environmental standards: Effectiveness on air pollutant emissions reduction. *J. Clean. Prod.* **2017**, *149*, 511–520. <https://doi.org/10.1016/j.jclepro.2017.02.127>.

71. Liu, X.J.; Xu, W.; Du, E.Z.; Tang, A.H.; Zhang, Y.; Zhang, Y.Y.; Wen, Z.; Hao, T.X.; Pan, Y.P.; Zhang, L.; et al. Environmental impacts of nitrogen emissions in China and the role of policies in emission reduction. *Philos. Trans. R. Soc. A* **2020**, *378*, 20190324. <https://doi.org/10.1098/rsta.2019.0324>.
72. Yuan, Q.; Qi, B.; Hu, D.; Wang, J.; Zhang, J.; Yang, H.; Zhang, S.; Liu, L.; Xu, L.; Li, W. Spatiotemporal variations and reduction of air pollutants during the COVID-19 pandemic in a megacity of Yangtze River Delta in China. *Sci. Total. Environ.* **2020**, *751*, 141820–141820. <https://doi.org/10.1016/j.scitotenv.2020.141820>.
73. Wu, C.; Lin, Z.; Shao, Y.; Liu, X.; Li, Y. Drivers of recent decline in dust activity over East Asia. *Nat. Commun.* **2022**, *13*, 7105. <https://doi.org/10.1038/s41467-022-34823-3>.
74. Jin, Y.; Ma, Y.; Zhang, M.; Liu, Y.; Lu, X.; Liu, B.; Jin, S.; Shen, A.; Zhang, J.; Fan, Q. Aerosol Characteristics during the COVID-19 Lockdown in China: Optical Properties, Vertical Distribution, and Potential Source. *Remote Sens.* **2022**, *14*, 3336. <https://doi.org/10.3390/rs14143336>.
75. Cao, J.J.; Wu, F.; Chow, J.C.; Lee, S.C.; Li, Y.; Chen, S.W.; An, Z.S.; Fung, K.K.; Watson, J.G.; Zhu, C.S.; et al. Characterization and source apportionment of atmospheric organic and elemental carbon during fall and winter of 2003 in Xi'an, China. *Atmospheric Meas. Technol.* **2005**, *5*, 3127–3137. <https://doi.org/10.5194/acp-5-3127-2005>.
76. Zhou, C.Y.; Liu, Q.; Tang, Y.; Wang, K.; Sun, L. Comparison between modis aerosol product c004 and c005 and evaluation of their applicability in the north of china. *J. Remote Sens.* **2009**, *13*, 854–872.
77. Wang, X.; Shen, Z.; Cao, J.; Zhang, L.; Liu, L.; Li, J.; Liu, S.; Sun, Y. Characteristics of surface ozone at an urban site of Xi'an in Northwest China. *J. Environ. Monit.* **2011**, *14*, 116–126. <https://doi.org/10.1039/c1em10541h>.

Disclaimer/Publisher's Note: The statements, opinions and data contained in all publications are solely those of the individual author(s) and contributor(s) and not of MDPI and/or the editor(s). MDPI and/or the editor(s) disclaim responsibility for any injury to people or property resulting from any ideas, methods, instructions or products referred to in the content.